

CERN-EP-2022-068

24 March 2022

Dielectron production at midrapidity at low transverse momentum in peripheral and semi-peripheral Pb–Pb collisions at $\sqrt{s_{\text{NN}}} = 5.02$ TeV

ALICE Collaboration*

Abstract

The first measurement of the e^+e^- pair production at low lepton pair transverse momentum ($p_{\text{T},ee}$) and low invariant mass (m_{ee}) in non-central Pb–Pb collisions at $\sqrt{s_{\text{NN}}} = 5.02$ TeV at the LHC is presented. The dielectron production is studied with the ALICE detector at midrapidity ($|\eta_e| < 0.8$) as a function of invariant mass ($0.4 \leq m_{ee} < 2.7$ GeV/ c^2) in the 50–70% and 70–90% centrality classes for $p_{\text{T},ee} < 0.1$ GeV/ c , and as a function of $p_{\text{T},ee}$ in three m_{ee} intervals in the most peripheral Pb–Pb collisions. Below a $p_{\text{T},ee}$ of 0.1 GeV/ c , a clear excess of e^+e^- pairs is found compared to the expectations from known hadronic sources and predictions of thermal radiation from the medium. The m_{ee} excess spectra are reproduced, within uncertainties, by different predictions of the photon–photon production of dielectrons, where the photons originate from the extremely strong electromagnetic fields generated by the highly Lorentz-contracted Pb nuclei. Lowest-order quantum electrodynamic (QED) calculations, as well as a model that takes into account the impact-parameter dependence of the average transverse momentum of the photons, also provide a good description of the $p_{\text{T},ee}$ spectra. The measured $\sqrt{\langle p_{\text{T},ee}^2 \rangle}$ of the excess $p_{\text{T},ee}$ spectrum in peripheral Pb–Pb collisions is found to be comparable to the values observed previously at RHIC in a similar phase-space region.

arXiv:2204.11732v2 [nucl-ex] 26 Jun 2023

1 Introduction

Ultra-relativistic heavy-ion collisions produce the largest electromagnetic (EM) fields experimentally accessible in the universe. The magnetic field generated by the highly Lorentz-contracted passing nuclei is predicted to reach up to 10^{15} Tesla [1]. Such strong EM fields are predicted to produce various exotic phenomena [2–5]. Heavy-ion collisions have therefore, in the past decades, induced a large amount of experimental and theoretical interest in the search for new aspects of quantum chromodynamics (QCD) and quantum electrodynamics (QED) [6–9].

The measurement of thermal dileptons from the quark–gluon plasma and the hot hadron gas produced in heavy-ion collisions has been long recognized as a clean and powerful probe to study the time evolution of the properties of the medium. Another important dilepton production mechanism, in particular at very low lepton pair transverse momentum ($p_{T,ll}$), is the photon–photon fusion process ($\gamma\gamma \rightarrow l^+l^-$). The EM fields surrounding the relativistic heavy ions with large charge number Z can be treated as a flux of quasi-real photons generated coherently, i.e. the charges of the Z protons in the nucleus act coherently leading to a Z^2 dependence of the quasi-real photon flux. Such photons, triggered by the EM fields of the two incoming nuclei, can interact via the Breit–Wheeler process [10] to produce dileptons. Such an exclusive photon-mediated process was first measured in ultra-peripheral heavy-ion collisions (UPC) by the STAR collaboration at RHIC [11]. Collisions with impact parameters (b) between the passing nuclei large enough that no nuclear overlap occurs can be selected, excluding any hadronic interaction. Only recently, the photon–photon production of dileptons has been observed in hadronic heavy-ion collisions (HHIC) by the STAR [12] and ATLAS [13, 14] collaborations. STAR measures dielectrons (e^+e^-) at midrapidity and small invariant mass m_{ee} ($0.4 \leq m_{ee} \leq 2.6$ GeV/ c^2) in non-central Au–Au and U–U collisions at a center-of-mass energy per nucleon pair of $\sqrt{s_{NN}} = 200$ GeV and 193 GeV, respectively, whereas ATLAS reports results on dimuon ($\mu^+\mu^-$) production at large $m_{\mu\mu}$ ($4 \leq m_{\mu\mu} < 45$ GeV/ c^2) in central, semi-central and peripheral Pb–Pb collisions at $\sqrt{s_{NN}} = 5.02$ TeV. The produced dileptons originate from quasi-real photons with momenta predominantly in the beam direction, i.e. the transverse component is of the order of ω_γ/γ_L , where ω_γ is the photon energy and γ_L is the Lorentz factor of the colliding nuclei. Therefore the lepton pairs have a very small $p_{T,ll}$ and the two leptons are nearly back-to-back. ATLAS quantifies the deviation from back-to-back in terms of the acoplanarity (α) defined as $1 - \frac{|\varphi^+ - \varphi^-|}{\pi}$ where φ^+ and φ^- are the azimuthal angles of the two muons. Both experiments show a significant broadening of the $p_{T,ee}$ (STAR) or α (ATLAS) distributions of the lepton pairs increasing for more central collisions in HHIC compared to UPCs. Whereas STAR attributed it to the possible deflection of the leptons by a magnetic field trapped in an electrically conducting QGP, ATLAS estimated that the observed broadening is qualitatively consistent with potential electromagnetic scatterings of the leptons with the hot and dense medium. Nevertheless, theoretical models tackling the relationship between b and the transverse momentum of the quasi-real photons were not readily available at the time of those results.

In the past, two main approaches have been used to calculate the photon–photon interactions: the Equivalent Photon Approximation (EPA) [15–17] and lowest-order QED calculations (LOQED) [18, 19]. In the EPA framework, the cross section of the two-photon process in heavy-ion collisions is obtained as a folding of the equivalent number of quasi-real photons $n_1(\omega_{\gamma,1})$ and $n_2(\omega_{\gamma,2})$ from the field of the nucleus 1 and 2, respectively, and the elementary photoproduction cross section $\sigma_{\gamma\gamma \rightarrow l^+l^-}$. The latter is given by the polarization-averaged cross section of the Breit–Wheeler process. Originally, the k_T -factorisation method as defined in Refs. [20, 21] was used to calculate the transverse momentum (k_T) of the quasi-real photons. In such an approach, the shape of the k_T -photon distribution is assumed to be independent of the collision impact parameter. Measurements of photon–photon produced dileptons by ALICE [22], CMS [23] and ATLAS [24] in UPCs are relatively well reproduced by calculations based on the EPA as implemented e.g. in STARlight [25]. Nevertheless, more differential measurements in UPCs show a broadening of the azimuthal back-to-back dilepton correlations or $p_{T,ll}$ distributions, as

well as differences in the invariant mass spectra with increasing number of neutrons at forward rapidity in the events [24, 26, 27]. The latter enables the selection of collisions occurring at small b that contain exclusive dileptons in conjunction with the excitation and dissociation of the passing nuclei. On one hand, ATLAS reported that their data can be described by EPA calculations using the k_T factorisation approach, as long as an additional, similarly factorized, dissociative contribution is included. In these dissociative processes, one photon is emitted by charged constituents of a nucleon, corresponding to an incoherent component of the photon fluxes. Its contribution was estimated by ATLAS by fitting the measured acoplanarity distributions [24]. On the other hand, CMS showed that their results for small α ($\alpha < 0.01 - 0.02$) can be qualitatively reproduced by LOQED calculations neglecting such dissociative processes but incorporating a b dependence of the shape of the initial photon k_T [27]. These calculations [28, 29] predict a k_T hardening of the initial-state photons with a decrease of b as a consequence of the spatial distribution of the EM fields. Attempts to implement b dependences in a generalized EPA approach have been performed in Refs. [28–31]. Such calculations show strong impact parameter dependences of the dilepton $p_{T,\parallel}$ distributions but produce an unphysical increase of the cross section at very low $p_{T,\parallel}$ [29], related to neglected interference terms. Recently, an approach using the Wigner formalism suggested in Ref. [32] and performed in Refs. [21, 33, 34], was shown to recover the full b dependence of the lowest-order QED calculations.

After including the b dependence of the photon k_T distribution in the calculations, the existing results of STAR [11, 12, 26], ATLAS [13, 14, 24], and CMS [27] in UPC and HHIC are reasonably well described by LOQED predictions and calculations based on the EPA within the uncertainties of the data. As a consequence, room for any medium-induced or final-state effect in HHIC is significantly reduced, whereas photon–photon interactions turn out to be useful for mapping the EM fields generated by the highly Lorentz-contracted nuclei. Further properties of the $\gamma\gamma \rightarrow e^+e^-$ process were measured by STAR. In particular, a $\cos(4\Delta\phi)$ angular modulation, where $\Delta\phi$ is the azimuthal angle in the laboratory frame between the momentum of the e^+e^- pair and one of the electrons, was predicted due to the initial linear photon polarization [32, 35]. This feature was confirmed by STAR measurements in UPCs and peripheral Au–Au collisions with hadronic overlap at $\sqrt{s_{NN}} = 200$ GeV/ c [26] and is closely related to the phenomenon of birefringence [36].

Despite the overall good description of the data by the latest calculations, some points deserve further theoretical and experimental investigation, see Ref. [37] for an overview. Among them, the effect of higher-order corrections in the QED predictions is unclear [38, 39]. Due to the large charge carried by the heavy ion, the parameter of the perturbative expansion in such calculations is large. The large tails observed in the measured $p_{T,ee}$ and α distributions could be related to next-leading-order contributions from final state radiation as shown in [27]. With ALICE, the $\gamma\gamma \rightarrow e^+e^-$ process can be studied in a similar region of phase space as measured by STAR, but in collisions with a much larger Lorentz-boost factor ($\gamma_L^{\text{LHC}} \approx 2700$, $\gamma_L^{\text{RHIC}} \approx 100$). The maximum electric field reached in heavy-ion collisions is of the order of $Ze\gamma/d^2$ [38], where d the distance from the ion’s center, and is consequently about 30 times larger at the LHC compared to RHIC. The fields vary and act over a short timescale of approximately $d/(\gamma_L c)$, i.e. 10^{-25} (10^{-23}) s at the LHC (RHIC). Therefore, measurements of photon–photon production of dielectrons at the LHC would allow the predicted photon kinematic distributions to be experimentally verified for larger expected magnetic fields than at RHIC and could provide further constraints on the mapping of the EM fields produced in heavy-ion collisions, as well as possible medium effects.

In this article, the first measurement of e^+e^- pairs at low $p_{T,ee}$ and m_{ee} at the LHC is presented in peripheral (70–90%) and semi-peripheral (50–70%) Pb–Pb collisions at $\sqrt{s_{NN}} = 5.02$ TeV. The dielectron production is measured with ALICE at midrapidity ($|\eta_e| < 0.8$) and $p_{T,ee} < 0.1$ GeV/ c from an invariant mass of 2.7 GeV/ c^2 down to 0.4 GeV/ c^2 . The latter is determined by the minimum p_T required to identify electrons ($p_{T,e} > 0.2$ GeV/ c) in the central barrel. The data are compared with the expected dielectron rate from known hadron decays, called the hadronic cocktail, with predictions for thermal radiation from

the medium and with recent predictions for coherent photoproduction of dielectrons as a function of m_{ee} . The $p_{T,ee}$ and $p_{T,ee}^2$ distributions are extracted in three different m_{ee} ranges in peripheral Pb–Pb collisions and the extracted value of $\sqrt{\langle p_{T,ee}^2 \rangle}$ is compared with predictions and to measurements at lower $\sqrt{s_{NN}}$.

The article is organized as follows. Section 2 contains a brief description of the ALICE apparatus and the data sample used, whereas Section 3 illustrates the analysis steps. In Section 4, the results on dielectron production yields at low $p_{T,ee}$ within the ALICE acceptance are presented and compared with theoretical calculations and previous measurements at lower $\sqrt{s_{NN}}$. Section 5 gives a summary and outlook.

2 Detector and data samples

A detailed description of the ALICE apparatus and its performance can be found in Refs. [40, 41]. The main detectors used to track and identify electrons¹ at midrapidity ($|\eta_e| < 0.8$) are the Inner Tracking System (ITS) [42], the Time Projection Chamber (TPC) [43], and the Time-Of-Flight (TOF) detector [44]. The ITS consists of six cylindrical layers of silicon detectors, which provide tracking of the charged particles and, together with the TPC, the reconstruction of the primary collision vertex. The innermost layer is installed at a radius of 3.9 cm from the beam axis and is used to reject electrons from photon conversions in the detector material. The TPC detector allows tracks to be reconstructed and charged particles to be identified (PID) via the measurement of the specific energy loss dE/dx while the TOF detector contributes to the PID via the measurement of the flight time of the particles. These detectors are placed inside a uniform magnetic field of 0.5 T parallel to the beam direction, provided by a solenoid magnet.

The data samples used in this analysis were collected by ALICE in 2015 and 2018 during Pb–Pb runs at $\sqrt{s_{NN}} = 5.02$ TeV. Minimum-bias collisions were triggered by requiring the coincidence of signals in the two scintillator arrays of the V0 detectors [45], covering the pseudorapidity ranges $2.8 \leq \eta < 5.1$ and $-3.7 \leq \eta < -1.7$. The time information from the V0 detectors and the neutron Zero Degree Calorimeters (ZDC) [46], as well as the correlation between the number of hits in the ITS and in the TPC are used offline to reduce the background from beam–gas interactions and pile-up collisions to a negligible level. Only events with a primary vertex reconstructed close to the center of ALICE along the beam direction ($|z| < 10$ cm) are considered in the analysis to assure a uniform detector acceptance. The event sample was divided into centrality classes [47] expressed in percentages of the total hadronic cross section using the amplitudes of the signal in the V0 detector. The number of events in each centrality class considered in this analysis, i.e. 50–70% and 70–90%, is about 34 million after the event selection criteria.

3 Data analysis

3.1 Electron candidate selection

Electron candidates are selected from charged-particle tracks reconstructed in the ITS and TPC in the kinematic range $|\eta_e| < 0.8$ and $p_{T,e} > 0.2$ GeV/ c . The track fits are required to include at least 80 out of a maximum of 159 reconstructed space points in the TPC and a hit in at least 4 of the 6 ITS detector layers. The χ^2 per space point measured in the TPC (ITS) must be less than 2.5 (5). In order to reduce the contribution of secondary tracks arising from weak decays and interactions with the detector material, only tracks with a distance-of-closest approach to the reconstructed primary vertex smaller than 1 cm in the plane transverse to the colliding beams and 0.5 cm in the longitudinal direction are used in the analysis. In addition, a hit in the first ITS layer is required to reject electrons originating from real-photon conversions in the detector material of the subsequent ITS layers. Since the electrons originating from the same photon conversion share the same cluster in the ITS layer where they are produced, they

¹Note that the term ‘electron’ is used for both electrons and positrons throughout this paper.

can be further suppressed by requiring that a maximum of one ITS cluster attached to the reconstructed track is shared with any other track candidate and is not placed in the first ITS layer.

The electron identification is based on the complementary information provided by the TPC and TOF. The detector PID signal, $n(\sigma_i^{\text{DET}})$, is expressed in terms of the deviation between the measured and expected value of the specific ionisation energy loss in the TPC or time-of-flight in the TOF for a given particle hypothesis i and momentum, normalised to the respective detector resolution. In the TPC, electrons are selected in the range $|n(\sigma_e^{\text{TPC}})| \leq 3$, whereas kaons, protons and pions are rejected with $|n(\sigma_K^{\text{TPC}})| \geq 3$, $|n(\sigma_p^{\text{TPC}})| \geq 3$ and $n(\sigma_\pi^{\text{TPC}}) \geq 3.5$, respectively. Electrons with an energy loss in the TPC in the range where the charged kaon and proton bands cross the one of electrons are recovered using the TOF information: tracks which fulfill only the TPC electron selection and pion rejection but have an associated TOF signal with $|n(\sigma_e^{\text{TOF}})| \leq 3$ are accepted. This PID strategy was used successfully in previous ALICE dielectron analyses in pp and p–Pb collisions [48–50]. Averaged over p_T , the hadron contamination in the single-electron candidate sample is less than 5% for an electron efficiency of about 80%. The largest hadron contamination, up to about 18% in the 50–70% centrality class, is observed where kaons ($p_T \approx 0.5$ GeV/ c), protons ($p_T \approx 1$ GeV/ c), or charged pions ($p_T > 6$ GeV/ c) have a similar dE/dx as electrons in the TPC. Pairs containing a misidentified hadron are further removed during the subtraction of the combinatorial background, thus that the final hadron contamination in the dielectron signal is expected to be negligible.

3.2 Signal extraction

Electron pairs originating from the same source cannot be identified unambiguously. Therefore, a statistical approach is used to extract the yield of signal pairs (S), in which all electrons and positrons in an event are combined to create an opposite charge-sign spectrum (OS). The combinatorial background (B) is estimated from same-event pairs with the same charge sign (SS). In comparison to a mixed-event approach [51], the same charge-sign approximation of the combinatorial background has the advantage to be self-normalized and to contain all residual correlations arising from charge-symmetric processes, such as from conversions of correlated decay photons originating from the same and from decays of different hadrons inside the same jets or in back-to-back jets. A different acceptance for opposite charge-sign and same charge-sign pairs is observed arising from detector geometrical effects, i.e. non-uniformity of the detector performances in azimuthal angle ϕ . The correction factor R_{acc} , needed to account for this effect, is calculated with an event-mixing technique detailed in Ref. [52]. Events with similar global properties are grouped together according to the z -position of the reconstructed primary vertex, the centrality of the collision, and the event-plane angle estimated with the V0 detector. The factor R_{acc} is found to be consistent with unity above m_{ee} of 1 GeV/ c^2 . The signal is then extracted as $S = OS - R_{\text{acc}} \times SS$.

The opposite charge-sign spectrum, the combinatorial background, and the extracted raw dielectron signal are shown in the left panel of Fig. 1 as a function of the pair transverse momentum $p_{T,ee}$ for $0.7 \leq m_{ee} < 1.1$ GeV/ c^2 in 70–90% peripheral Pb–Pb collisions. The corresponding signal-over-background ratio (S/B) is presented in the right panel of Fig. 1. Towards very low $p_{T,ee}$ ($p_{T,ee} \leq 0.1$ GeV/ c), the S/B ratio increases for both centrality classes. However, the S/B ratio is about one order of magnitude lower in the 50–70% centrality class in this $p_{T,ee}$ region.

3.3 Efficiency correction

The raw signal is corrected for the finite dielectron reconstruction efficiency. To this end, different Monte Carlo (MC) simulations are used, where a realistic detector response is modelled using GEANT3 [53]. For very low $p_{T,ee}$ ($p_{T,ee} < 0.2$ GeV/ c), photoproduced e^+e^- pairs are simulated with the event generator STARlight [25] and embedded into hadronic collisions computed with HIJING [54]. At larger $p_{T,ee}$, additional samples of dielectron sources injected into HIJING simulated events are utilized. These include light-flavour hadrons (π^0 , η , η' , ρ^0 , ω and ϕ) and J/ψ mesons, forced to decay into dielectrons with

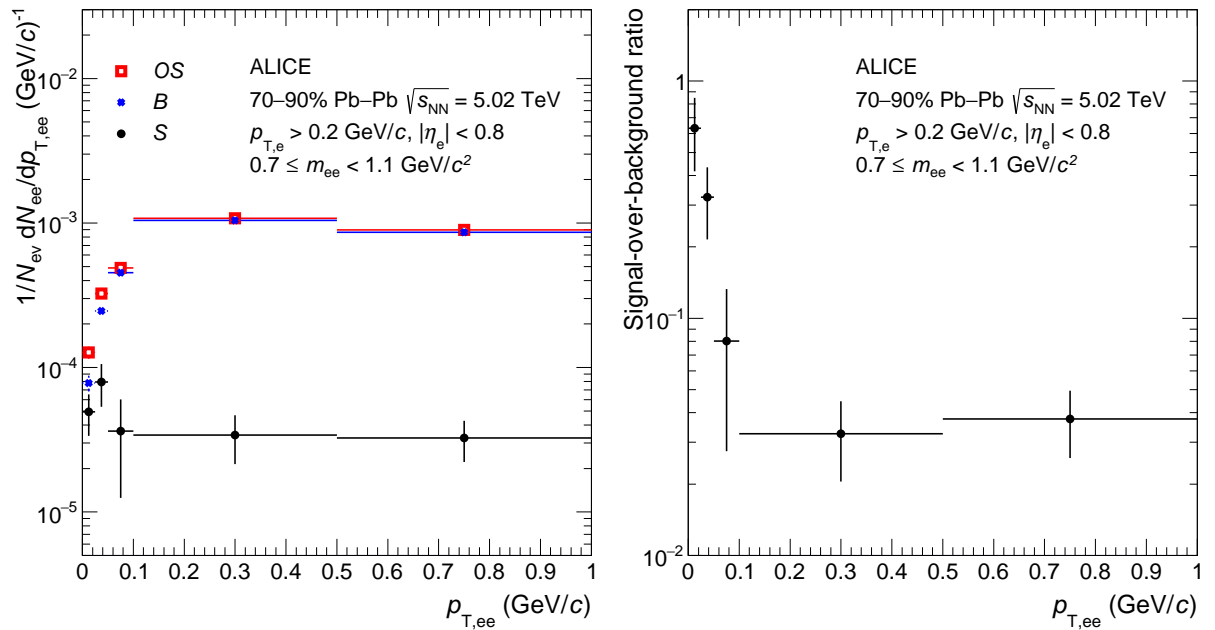


Figure 1: Left panel: raw $p_{T,ee}$ -differential yield (S) in peripheral (70–90%) Pb–Pb collisions at $\sqrt{s_{NN}} = 5.02$ TeV for $0.7 \leq m_{ee} < 1.1$ GeV/ c^2 overlaid with the opposite charge-sign distribution (OS) and the same charge-sign spectrum multiplied by the acceptance correction factor R_{acc} (B). Right panel: signal over background as a function of $p_{T,ee}$ in peripheral (70–90%) Pb–Pb collisions at $\sqrt{s_{NN}} = 5.02$ TeV for $0.7 \leq m_{ee} < 1.1$ GeV/ c^2 .

the phenomenological EXODUS generator [51] and PHOTOS [55], respectively, and produced in equal amounts with uniform p_T distributions. In each centrality class (50–70% or 70–90%), these input p_T distributions are corrected with p_T -dependent weights defined as the ratio of the hadron p_T spectra in the MC simulations and the expected hadron p_T distributions according to the hadronic cocktail explained in Section 3.5. The weights are passed to the decay electrons to produce a realistic mix of e^+e^- pairs from the various sources considered. In addition, an enriched sample of heavy-flavour hadron sources with enforced semileptonic decay channels generated with the Perugia 2011 tune of PYTHIA 6.4 [56, 57] is used. The final efficiency as a function of m_{ee} and $p_{T,ee}$ is the average of the efficiencies of the different dielectron sources, weighted by their expected contribution, for $p_{T,ee} \geq 0.2$ GeV/ c . At lower $p_{T,ee}$ only the STARlight calculations are taken as input. Other sources show dielectron efficiencies in agreement within statistical uncertainties with the one extracted for e^+e^- pairs produced via photon–photon interactions.

3.4 Systematic uncertainties of measured dielectron spectra

The systematic uncertainties on the measured $p_{T,ee}$ - and m_{ee} -differential dielectron yields in peripheral (70–90%) and semi-peripheral (50–70%) collisions originate from tracking, electron identification and purity, and background subtraction. They are evaluated as described in Ref. [48] and summarised in Table 1 for $p_{T,ee} < 0.1$ GeV/ c .

The systematic uncertainties related to the requirement of a hit in the innermost ITS layer, the matching of the TPC track and the signal measured in the TOF, and the matching of the track segments reconstructed in the ITS and the TPC are first estimated at the single-track level. To this end, the efficiencies of these selection criteria are compared in data and in MC as a function of p_T for a pure sample of charged pions or electrons (TPC–TOF matching). The latter is obtained by selecting electrons from photon conversions in the detector material using topological requirements. A MC method is then used to calculate the corresponding uncertainties for dielectrons, by generating particles in the full m_{ee} and $p_{T,ee}$

Table 1: Summary of the total systematic uncertainties of the measured dielectron yields for $p_{T,ee} < 0.1$ GeV/ c in semi-peripheral (50–70%) and peripheral (70–90%) Pb–Pb collisions at $\sqrt{s_{NN}} = 5.02$ TeV. The values presented as a range correspond to the smallest and largest observed systematic uncertainties.

Centrality class	Hit in the first ITS layer	TPC–TOF matching	ITS–TPC matching	Shared ITS cluster	Tracking and PID	Anchor point	Total
50–70%	2%	0–4%	5.4–7.4%	4%	16%	0%	18%
70–90%	2%	0–4%	5.4–7.4%	4%	6%	5%	10–12%

phase space and forcing them to decay to e^+e^- pairs. The uncertainty for each e^+e^- pair is given by the sum of the uncertainties of the decay electrons, after applying the fiducial selection ($|\eta_e| < 0.8$ and $p_{T,e} \geq 0.2$ GeV/ c). The final systematic uncertainty is obtained after averaging for a given m_{ee} and $p_{T,ee}$ over all generated particles. The TPC–TOF matching efficiency is relevant only in the regions where the kaon and proton bands cross the band of electrons in the TPC. The corresponding uncertainty varies between 0 and 4% for the e^+e^- pairs and is the largest for the invariant mass bin $1.1 \leq m_{ee} < 2.7$ GeV/ c^2 at low $p_{T,ee}$ ($p_{T,ee} < 0.1$ GeV/ c). The ITS–TPC matching efficiency is one of the dominant sources of systematic uncertainties together with the particle identification and leads to uncertainties between 5.4% and 7.4% increasing with m_{ee} . The systematic uncertainty originating from the requirement of a hit in the first ITS layer is of the order of 2%.

The systematic uncertainty from the requirement on the number of ITS shared clusters is estimated by varying the number of allowed shared ITS clusters for the selected electron candidates and repeating the analysis steps. Releasing completely this selection criterion increases significantly the amount of electrons from conversions in the detector material and leads to a smaller S/B by a factor of about 0.6. Therefore the extracted systematic uncertainty contains not only systematic effects from the signal efficiency, but also from the background estimation. It is calculated from the maximum deviations of the efficiency-corrected spectra variations, considered as statistically significant according to the Barlow criterion [58] and found to be of the order of 4%.

In a similar way, the systematic uncertainty arising from the tracking and electron identification and purity is evaluated by varying the remaining electron selection criteria simultaneously, e.g. the requirement on the minimum number of reconstructed space points in the TPC or $|n(\sigma_e^{\text{TPC}})|$, to take into account possible correlations between them. In particular modifying the requirements on the TPC and TOF signals, i.e. $|n(\sigma_e^{\text{TPC}})|$, $|n(\sigma_\pi^{\text{TPC}})|$, $|n(\sigma_K^{\text{TPC}})|$, $|n(\sigma_p^{\text{TPC}})|$ and $|n(\sigma_e^{\text{TOF}})|$, enables to probe possible biases due to differences in the detector responses in data and MC and remaining hadron contamination in the electron sample. The systematic uncertainty is computed as the root-mean-square of the variation of the final data points and is found to be of the order of 16% (6%) in semi-peripheral (peripheral) Pb–Pb collisions for $p_{T,ee} < 0.1$ GeV/ c . The main source of systematic uncertainty in the 50–70% centrality class comes from the kaon and proton rejection in the TPC and the non-perfect description of the measured particle energy loss in the TPC in the simulations, which depends on the centrality of the collisions.

The systematic uncertainty originating from the correction factor R_{acc} , estimated by varying the event mixing pools used to calculate it, was found to be negligible at low $p_{T,ee}$.

Finally, systematic uncertainties arise from the centrality class definition. The absolute scale of the centrality is defined by the range of 0–90% centrality in which a Glauber-based multiplicity model is fitted to the VOM distribution [47]. The lower centrality limit of 90% of this range with its corresponding VOM signal is denoted the anchor point (AP). The AP was shifted by $\pm 1\%$, leading to a systematic uncertainty of 5% for the 70–90% centrality class and negligible for the 50–70% centrality class.

3.5 Expected yield from known hadronic sources

The expected dielectron yield from the decays of known hadrons produced in the hadronic Pb–Pb collisions, called the hadronic cocktail, is calculated with a fast simulation of the ALICE central barrel, including the angular and momentum resolution of the detector and bremsstrahlung effects [59].

The Dalitz and dielectron decays of light neutral mesons are simulated following the approach described in Ref. [60]. The p_T -differential production cross sections of η and ω are estimated based on the ratio of their p_T spectra to the one of π^0 or π^\pm , measured in different collision systems and at different center-of-mass energies, whereas η' , ρ , and ϕ are generated assuming m_T -scaling over the full p_T range or only at low p_T [61–63]. The p_T spectra of π^\pm , measured down to a p_T of 0.1 GeV/c as a function of the collision centrality in Pb–Pb collisions at $\sqrt{s_{NN}} = 5.02$ TeV [64], are parametrized and extrapolated to $p_T = 0$ using a two-component function [65, 66]. The difference between π^0 and π^\pm due to isospin-violating decays is taken into account using an effective model that describes measured hadron spectra (π^\pm , K^\pm , and p [64]) at low p_T and includes strong and electromagnetic decays [67], as described in Ref. [49]. This leads to p_T -dependent scaling factors applied to the π^\pm parametrizations of about 1.3 for $p_T \rightarrow 0$ and consistent with unity within 2% for $p_T > 1$ GeV/c. The p_T spectrum of η is computed as the average of the spectra obtained using the parametrizations retrieved from the η/π^0 ratio as a function of p_T in pp collisions [49] and from the K^\pm/π^\pm ratio as a function of p_T measured down to $p_T = 0.3$ GeV/c in Pb–Pb collisions [64]. In all considered centrality classes (50–70% and 70–90%), the ratio of the resulting p_T distribution of η to the π^0 parametrization at very low p_T ($p_T \leq 0.1$ GeV/c) was found to be in agreement within uncertainties with the η/π^0 ratio in pp collisions. The latter is constrained at low p_T by the data from CERES/TAPS [68] and has a conservative p_T -dependent uncertainty of up to 40%, which is taken into account in the final uncertainty of the hadronic cocktail. At m_{ee} around 0.782 GeV/c², the dominant contribution to the hadronic cocktail is given by the ω meson. A parametrization of the ω/π^0 ratio as a function of p_T measured by ALICE in pp collisions at $\sqrt{s} = 7$ TeV [69] is performed and extended to $p_T = 0$ using data from PHENIX in pp collisions at $\sqrt{s} = 200$ GeV [70]. It is used for all centrality classes. Finally, the measured p_T spectra of ϕ mesons in semi-central and peripheral Pb–Pb collisions at $\sqrt{s_{NN}} = 5.02$ TeV [71] are fitted and extrapolated down to low p_T ($p_T \leq 0.4$ GeV/c) using m_T scaling to obtain the ϕ input parametrizations.

The contribution from correlated semileptonic decays of open charm and beauty hadrons is computed with the next-to-leading order event generator POWHEG [72–75] with PYTHIA 6 [56] to evolve the parton shower. The expected yield is normalized to the cross sections $d\sigma_{c\bar{c}}/dy|_{y=0}$ and $d\sigma_{b\bar{b}}/dy|_{y=0}$ extracted with the same MC generator from the e^+e^- spectra measured in pp collisions at $\sqrt{s} = 5.02$ TeV [48] and scaled with the nuclear overlap function. The resulting contribution from correlated open heavy-flavour hadron decays dominates the hadronic cocktail yield for $p_{T,ee} < 0.1$ GeV/c up to m_{ee} of 2.7 GeV/c², except in the mass regions around 0.4, 0.78 and 1. GeV/c², where the η , ω and ϕ are the main sources of e^+e^- pairs, respectively. The uncertainties related to the branching ratio of the semileptonic decays of the open heavy-flavour hadrons and the fragmentation functions of charm and beauty quarks are omitted under the assumption that these do not change from pp to peripheral and semi-peripheral Pb–Pb collisions.

The systematic uncertainties of the hadronic cocktail are computed by adding in quadrature the uncertainties originating from the following sources: the π^\pm and ϕ parametrizations as a function of p_T , the π^0/π^\pm correction factor, the η/π^0 and ω/π^0 ratios, the m_T -scaling parameters used for η' , ρ and ϕ , the branching ratios of the different light-flavour hadron decay channels, the heavy-flavour cross sections and the nuclear overlap function. The final systematic uncertainty of the hadronic cocktail at very low p_T ($p_{T,ee} < 0.1$ GeV/c) is between 14% in the intermediate mass range ($1.1 \leq m_{ee} < 2.7$ GeV/c²) and about 30% in the mass regions dominated by η and ω decays.

4 Results

4.1 Invariant mass spectra

The efficiency-corrected e^+e^- invariant mass spectra at low $p_{T,ee}$ ($p_{T,ee} < 0.1$ GeV/ c) are shown in Fig. 2 in peripheral (70–90%) and semi-peripheral (50–70%) Pb–Pb collisions at $\sqrt{s_{NN}} = 5.02$ TeV within the ALICE acceptance ($|\eta_e| < 0.8$ and $p_{T,e} > 0.2$ GeV/ c). In this figure and the following ones, the upper limit at 90% C.L. using the Feldman and Cousins methodology [76] is reported for the results which are found to be statistically consistent with zero within one standard deviation. The data are compared with cocktails of expected e^+e^- hadronic sources. The corresponding enhancement factors, expressed as ratios of data over hadronic cocktail, are illustrated in the bottom panel of Fig. 2. The total uncertainty of the cocktail is represented by a band. An excess of dielectrons compared to the hadronic expectation is observed in both centrality classes, with a larger significance in peripheral Pb–Pb collisions.

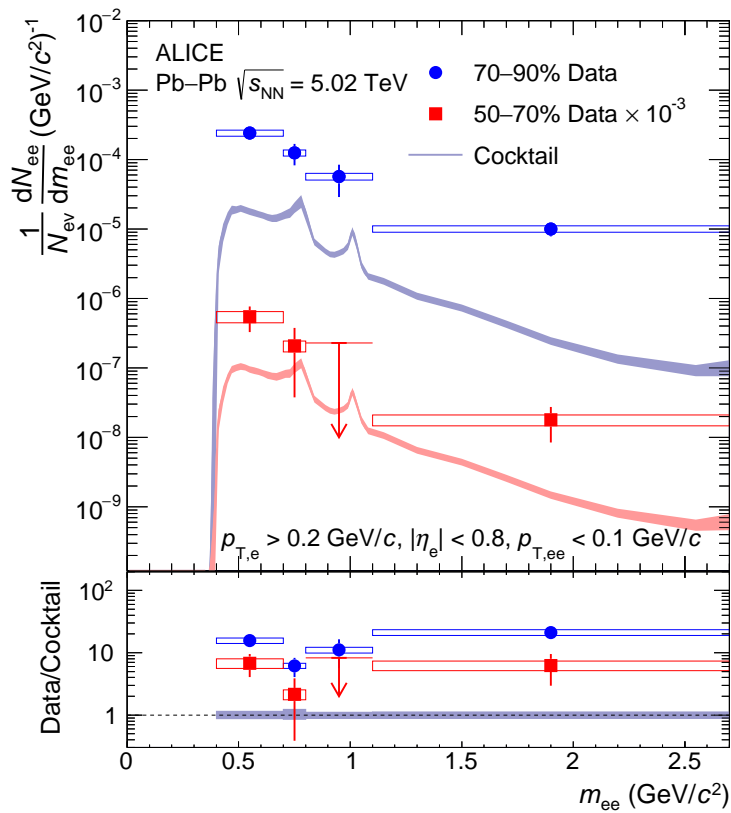


Figure 2: Dielectron m_{ee} -differential yields in semi-peripheral (50–70%) and peripheral (70–90%) Pb–Pb collisions at $\sqrt{s_{NN}} = 5.02$ TeV, compared with the expected e^+e^- contributions from known hadronic decays. The error bars and boxes represent the statistical and systematic uncertainties of the data, respectively, whereas the bands show the uncertainties of the hadronic cocktail. Arrows indicate upper limits at 90% confidence level.

The hadronic cocktail contribution is subtracted from the inclusive e^+e^- pairs to obtain the invariant mass distributions for excess e^+e^- pairs with $p_{T,ee} < 0.1$ GeV/ c presented in the left and right panels of Fig. 3 for the 50–70% and 70–90% centrality classes, respectively. The yield of excess e^+e^- pairs does not show a significant centrality dependence. The expected contributions from thermal dielectrons from the partonic and hadronic phases are also shown in the figure. They are estimated with an expanding thermal fireball model including an in-medium broadened ρ spectral function [77–79]. Predictions from the same model describe well the SPS [80, 81] and RHIC [82, 83] data. At $p_{T,ee} < 0.1$ GeV/ c , thermal radiation from the medium is expected to be at least one order of magnitude smaller than the measured e^+e^-

excess in peripheral Pb–Pb collisions and have a different $p_{T,ee}$ shape and centrality dependence [20]. The excess yield in the e^+e^- invariant mass spectra are further compared with different calculations for photon–photon production of dielectrons. A QED calculation at leading-order was performed by the authors of Refs. [29, 37]. The lowest-order two-photon interaction is a second-order process with two contributing Feynman diagrams, as shown in Fig. 2 of Ref. [18]. Higher-order contributions are ignored, although the parameter of the perturbative expansion, the coupling $Z\alpha$ with α the fine structure constant, is close to unity, i.e. 0.6, for lead ions. The straight-line approximation for the incoming projectile and target nuclei is applied, as for the other calculations. The predictions from the authors of Ref. [21] employ the Wigner formalism. The quasi-real photon fluxes originating from strong EM fields produced by the highly Lorentz-contracted heavy ions passing each other can be written in terms of Wigner functions in momentum and impact-parameter space. The cross section for the $\gamma\gamma \rightarrow e^+e^-$ process is then expressed as a convolution over impact parameters and transverse momenta. Realistic charge form factors of the Pb nuclei, i.e. Fourier transforms of the charge density, are taken from Ref. [84]. About 50% of the e^+e^- pairs are produced inside the nuclei for the centrality class 70–90%. The model implemented in the STARlight MC generator uses the equivalent photon approximation approach [25, 85]. The main difference between STARlight and the two aforementioned calculations is related to the treatment of the b dependence in the computations. STARlight utilizes the k_T -factorisation method, where the one-photon distribution is integrated over all transverse distances to obtain the shape of the k_T distribution. For all models, the m_{ee} and $p_{T,ee}$ detector resolution, not corrected in the data, are taken into account by folding the momentum and opening angle resolution, including bremsstrahlung effects, in the calculations. As a result, the predicted m_{ee} distributions are slightly softer than the ones computed with perfect detector resolution. The magnitude of the effect is nevertheless below the sensitivity of the data. All models can reproduce the measured m_{ee} excess spectra within their uncertainties. The ratios of the measured excess yields to the different calculations, shown in the bottom panels of Fig. 3, are consistent with unity within the statistical and systematic uncertainties of the data in both centrality classes. However, the STARlight predictions appear to be further away from the data than the other calculations. The contributions from decays of vector mesons produced in photo–nuclear collisions are expected to be very small for ρ , ω and ϕ [12, 26] and below 5% based on ALICE results for photoproduced J/ψ at forward rapidity in Pb–Pb collisions at $\sqrt{s_{NN}} = 5.02$ TeV [86] extrapolated to midrapidity using the IIM model scenario 2 in Ref. [87].

4.2 Transverse momentum spectra

In order to further investigate the dielectrons produced via photon–photon interactions at low $p_{T,ee}$, the $p_{T,ee}$ spectra of inclusive e^+e^- pairs are shown in three different invariant mass ranges in peripheral Pb–Pb collisions at $\sqrt{s_{NN}} = 5.02$ TeV in Fig. 4. While the measured yield at $p_{T,ee} \geq 0.1$ GeV/c can be described by the hadronic cocktail, a clear peak is seen at $p_{T,ee}$ smaller than 0.1 GeV/c in all m_{ee} ranges. The latter is fairly well reproduced by the aforementioned photon–photon models including the impact parameter dependence of the photon k_T distribution, i.e. the lowest-order QED calculations [29, 37] and calculations using the Wigner formalism [21]. Both approaches predict very similar $p_{T,ee}$ distributions. On the contrary, all spectra computed with the STARlight model [25, 85] show a rise towards $p_{T,ee}$ equal to zero, which is disfavored by the data. By integrating over all transverse distances in the single-photon distribution, the k_T -factorization approach employed in STARlight leads to a $p_{T,ee}$ distribution whose shape is independent of the impact parameter. Such a treatment gives rise to uncertainties on the k_T photon distribution of the order of ω_γ/γ_L , which is precisely the same order of magnitude as k_T itself [18, 30]. Therefore the b dependence of k_T , and as a consequence of $p_{T,ee}$, needs to be taken into account in the calculations in order to interpret the results correctly. The limited p_T resolution of the detector has a negligible effect compared to the data uncertainties at low m_{ee} ($0.4 \leq m_{ee} < 0.7$ GeV/c²) but it affects more significantly the reconstructed $p_{T,ee}$ distributions at large m_{ee} ($1.1 \leq m_{ee} < 2.7$ GeV/c²). At large m_{ee} , where electrons have larger p_T , the detector resolution on p_T worsens. The reconstructed $p_{T,ee}$ distributions are pushed towards larger $p_{T,ee}$ values compared to the true $p_{T,ee}$ spectra. The maximum of

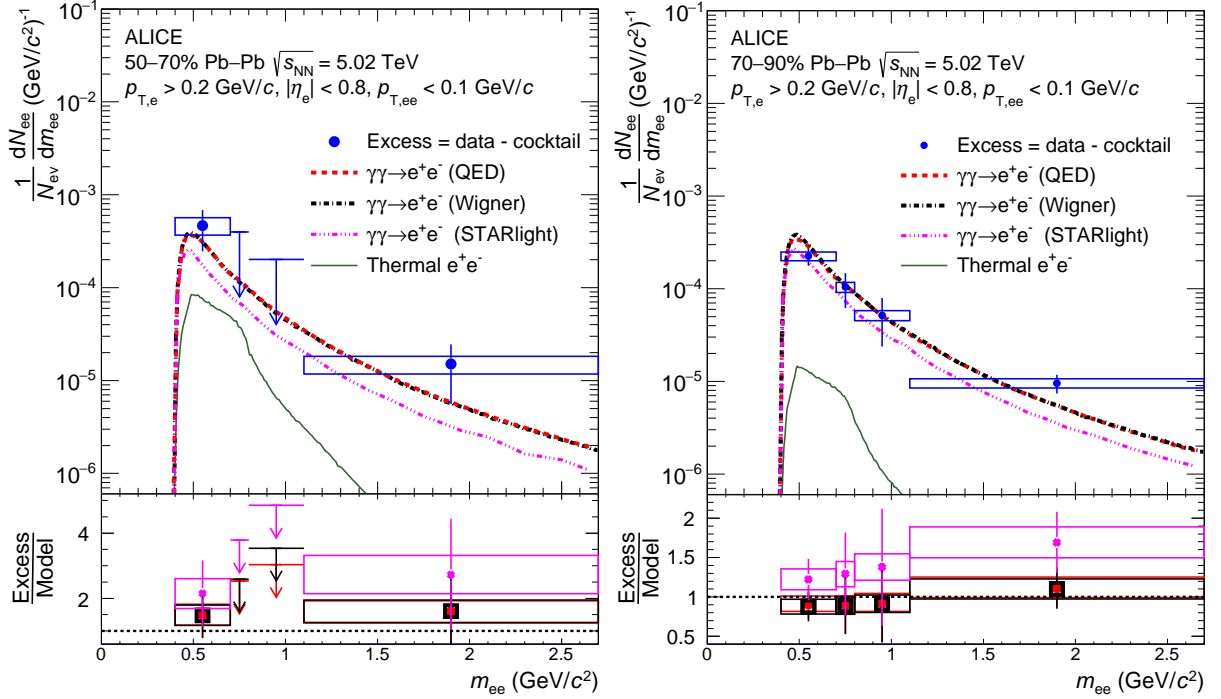


Figure 3: Excess dielectron m_{ee} -differential yields after subtraction of the cocktail of known hadronic decay contributions in semi-peripheral (left) and peripheral (right) Pb–Pb collisions at $\sqrt{s_{NN}} = 5.02$ TeV, compared with calculations for coherent two-photon production of e^+e^- pairs folded with the detector resolution [21, 25, 29, 37, 85]. For details see the text. The error bars and boxes represent the statistical and systematic uncertainties of the data, respectively. Arrows indicate upper limits at 90% confidence level.

the spectra predicted with the Wigner formalism and lowest-order QED calculations is reduced by about 35%.

The $p_{T,ee}^2$ distributions of the excess e^+e^- pairs after subtracting the hadronic cocktail are shown in Fig. 5 for the three invariant mass regions in peripheral Pb–Pb collisions at $\sqrt{s_{NN}} = 5.02$ TeV together with the different calculations for photon–photon production of dielectrons [21, 25, 29, 37, 85]. The data can be reproduced by the lowest-order QED predictions [29, 37] and computations from the authors of Ref. [21], whereas the STARlight calculation [25, 85] falls below the data points for $p_{T,ee}^2$ larger than 6.25×10^{-4} (GeV/c) 2 and overshoots the measured spectra at low $p_{T,ee}^2$. This observation is consistent with the results shown as a function of $p_{T,ee}$ and is in line with previous experimental measurements [24, 26, 27] which have demonstrated that the photon k_T -factorization approach used in STARlight lacks b dependences clearly visible in the experimental measurements. The data support the statement that the $p_{T,ee}$ broadening observed in HHICs in comparison to those in UPCs originates predominantly from the initial EM field strength that varies significantly with impact parameter. To quantify the spread of the $p_{T,ee}$ distributions, the $\sqrt{\langle p_{T,ee}^2 \rangle}$ is calculated for both the data and aforementioned photon–photon models in the measured $p_{T,ee}^2$ range ($0 \leq p_{T,ee}^2 < 0.01$ (GeV/c) 2). The values are given in Table 2. The measured $\sqrt{\langle p_{T,ee}^2 \rangle}$ are found to be in agreement with expectations from theory within uncertainties. The lowest-order QED calculations and the predictions based on the Wigner formalism predict similar $\sqrt{\langle p_{T,ee}^2 \rangle}$ for the three different m_{ee} bins. The increase observed in Table 2 is mostly due to detector p_T resolution effects. The data are not yet precise enough to conclude on a possible m_{ee} dependence of $\sqrt{\langle p_{T,ee}^2 \rangle}$.

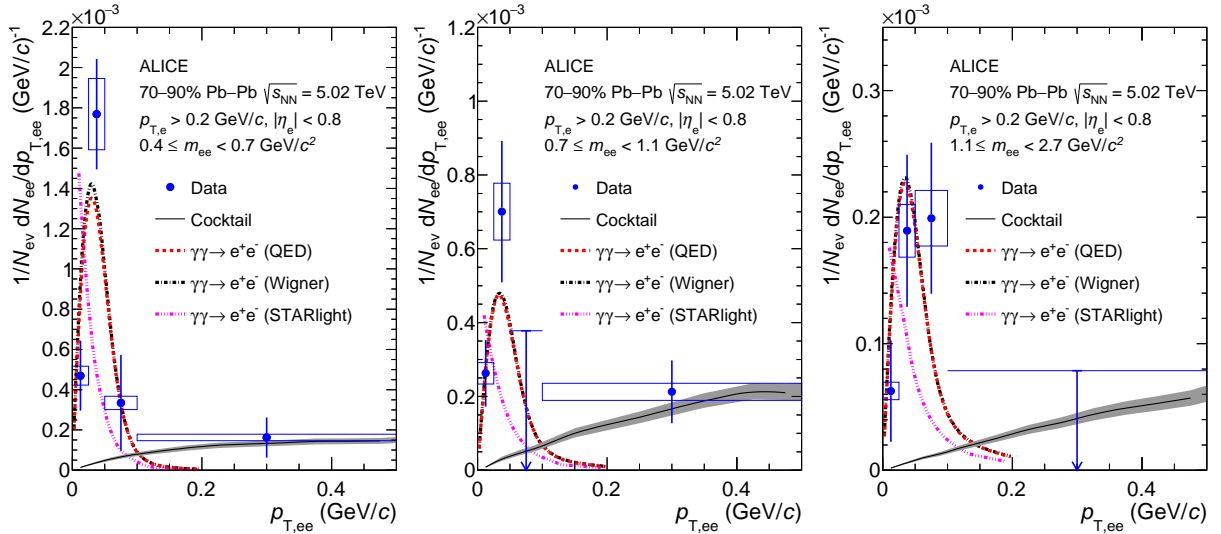


Figure 4: Dielectron $p_{T,ee}$ -differential yields in peripheral (70–90%) Pb–Pb collisions at $\sqrt{s_{NN}} = 5.02$ TeV for three different m_{ee} ranges, i.e. $0.4 \leq m_{ee} < 0.7$ GeV/ c^2 (left), $0.7 \leq m_{ee} < 1.1$ GeV/ c^2 (middle), and $1.1 \leq m_{ee} < 2.7$ GeV/ c^2 (right), compared with the expected e^+e^- contributions from known hadronic decays and calculations for coherent two-photon production of dielectrons folded with the detector resolution [21, 25, 29, 37, 85]. For details see the text. The error bars and boxes represent the statistical and systematic uncertainties of the data, respectively, whereas the bands show the uncertainties of the hadronic cocktail. Arrows indicate upper limits at 90% confidence level.

Table 2: The measured $\sqrt{\langle p_{T,ee}^2 \rangle}$ of excess yields in 70-90% peripheral Pb–Pb collisions at $\sqrt{s_{NN}} = 5.02$ TeV compared with expectations from photon–photon calculations [21, 25, 29, 37, 85]. For details see text.

Mass region (GeV/ c^2)	Data	QED [29, 37]	Wigner [21]	STARlight [25, 85]
$0.4 \leq m_{ee} \leq 0.7$	44 ± 28 (stat.) ± 6 (syst.) MeV/ c	44 MeV/ c	45 MeV/ c	30 MeV/ c
$0.7 \leq m_{ee} \leq 1.1$	45 ± 36 (stat.) ± 8 (syst.) MeV/ c	48 MeV/ c	48 MeV/ c	38 MeV/ c
$1.1 \leq m_{ee} \leq 2.7$	69 ± 36 (stat.) ± 8 (syst.) MeV/ c	50 MeV/ c	50 MeV/ c	42 MeV/ c

On the right panel of Fig. 5, the measured $p_{T,ee}^2$ spectrum for $0.4 \leq m_{ee} < 0.7$ GeV/ c^2 in peripheral Pb–Pb collisions is compared to the $p_{T,ee}^2$ distributions measured by the STAR collaboration in a similar phase-space region in peripheral (60–80%) Au–Au and U–U collisions at $\sqrt{s_{NN}} = 200$ GeV and 193 GeV [12]. On the one hand, the $\sqrt{s_{NN}}$ dependence of the cross section for the reaction $\gamma\gamma \rightarrow e^+e^-$ is expected to be rather small from RHIC to LHC energies in the low m_{ee} range and midrapidity region considered here [20]. On the other hand, the Z of the different colliding ions are different ($Z_{Au} = 79$, $Z_{Pb} = 82$, $Z_U = 92$) and the η_e , y_{ee} , and m_{ee} ranges used in the STAR and ALICE experiments are not exactly the same. The results at LHC are found to be similar to the ones at RHIC within large uncertainties. The measured $\sqrt{\langle p_{T,ee}^2 \rangle}$ (see Table 2) is comparable to the ones observed in peripheral Au–Au (50.8 ± 2.51 (stat.+syst.) MeV/ c) and U–U (43 ± 2.26 (stat.+syst.) MeV/ c) collisions.

5 Summary and outlook

The first measurements of e^+e^- pairs at low $p_{T,ee}$ ($p_{T,ee} < 0.1$ GeV/ c) and m_{ee} ($0.4 \leq m_{ee} < 2.7$ GeV/ c^2) at LHC energies are presented at midrapidity ($|\eta_e| < 0.8$) in peripheral (70–90%) and semi-peripheral (50–70%) Pb–Pb collisions at $\sqrt{s_{NN}} = 5.02$ TeV. An excess of dielectrons is observed at low $p_{T,ee}$ over the full

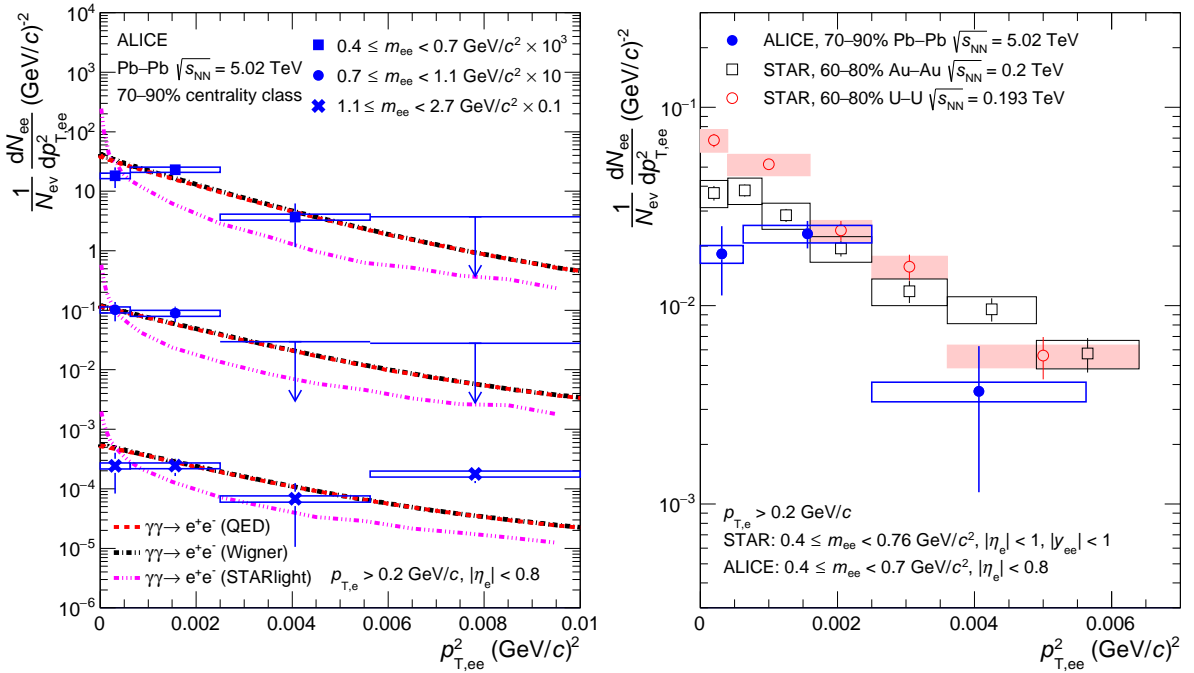


Figure 5: Left: Excess dielectron $p_{T,ee}^2$ -differential yields after subtraction of the cocktail of known hadronic decay contributions in peripheral (70–90%) Pb–Pb collisions at $\sqrt{s_{NN}} = 5.02$ TeV for different m_{ee} ranges, i.e. $0.4 \leq m_{ee} < 0.7$ GeV/ c^2 , $0.7 \leq m_{ee} < 1.1$ GeV/ c^2 and $1.1 \leq m_{ee} < 2.7$ GeV/ c^2 , compared with calculations for coherent photon–photon production of dielectrons folded with the detector resolution [21, 25, 29, 37, 85]. Right: Excess dielectron $p_{T,ee}^2$ -differential yields after subtraction of the cocktail of known hadronic decay contributions in peripheral Pb–Pb (70–90%), Au–Au (60–80%) and U–U (60–80%) collisions at $\sqrt{s_{NN}} = 5.02$, 0.2 and 0.193 TeV [12], respectively, in a similar m_{ee} range. The error bars and boxes represent the statistical and systematic uncertainties of the data, respectively. Arrows indicate upper limits at 90% confidence level.

measured m_{ee} range compared to the expected e^+e^- yield from known hadronic sources and thermal radiation from the medium in Pb–Pb collisions. The excess yields after subtraction of the hadronic cocktail do not exhibit a significant centrality dependence and can be reproduced as a function of m_{ee} by different calculations for photon–photon production of dielectrons in both centrality classes. In peripheral Pb–Pb collisions the inclusive $p_{T,ee}$ spectra and the excess dielectron $p_{T,ee}^2$ distributions are shown in three different m_{ee} intervals ($0.4 \leq m_{ee} < 0.7$ GeV/ c^2 , $0.7 \leq m_{ee} < 1.1$ GeV/ c^2 , and $1.1 \leq m_{ee} < 2.7$ GeV/ c^2) and compared with the hadronic cocktail and predictions for the $\gamma\gamma \rightarrow e^+e^-$ process using the same models as for the m_{ee} spectra. The results at $p_{T,ee} < 0.1$ GeV/ c ($p_{T,ee}^2 < 0.01$ (GeV/ c) 2) clearly disfavor the shape of the spectra of photon–photon produced dielectrons computed with STARlight [25, 85], whereas they are reproduced by lowest-order QED calculations [29, 37] and calculations using the Wigner formalism [21]. STARlight does not contain any impact-parameter effects on the shape of the transverse momentum distribution of the quasi-real photons and thus on the one of the $p_{T,ee}$ and $p_{T,ee}^2$ distributions of the produced e^+e^- pairs. According to the calculations [21, 25, 29, 37, 85], these impact-parameter dependencies cannot be neglected in theoretical models computing the $\gamma\gamma \rightarrow l^+l^-$ process in non ultra-peripheral heavy-ion collisions in order to interpret the data correctly. These results are in line with the statement that the $p_{T,ee}$ broadening observed in HHICs in comparison to those in UPCs originates predominantly from the initial electromagnetic field strength that varies significantly with impact parameter. Therefore, determining precisely the magnitude of possible final-state effects related to the creation of a hot and dense medium in HHICs requires a very good understanding of the electromagnetic field produced in heavy-ion collisions. Finally, the measured $\sqrt{\langle p_{T,ee}^2 \rangle}$ in $0.4 \leq m_{ee} < 0.7$ GeV/ c^2 is compatible

with the values observed in non-central Au–Au and U–U collisions by STAR at RHIC [12].

A significant improvement in the measurement, as well as more differential studies, are expected after the ALICE upgrades for the LHC Runs 3 and 4, where the number of recorded collisions for the centrality classes considered in this article is expected to increase by a factor greater than 50 [88–90]. The reduced material budget in front of the first tracking layer, together with the improved resolution of the distance-of-closest approach to the collision vertex, will help to suppress the combinatorial and heavy-flavour backgrounds, relevant in such analyses.

Acknowledgements

The ALICE Collaboration would like to thank all its engineers and technicians for their invaluable contributions to the construction of the experiment and the CERN accelerator teams for the outstanding performance of the LHC complex. The ALICE Collaboration gratefully acknowledges the resources and support provided by all Grid centres and the Worldwide LHC Computing Grid (WLCG) collaboration. The ALICE Collaboration acknowledges the following funding agencies for their support in building and running the ALICE detector: A. I. Alikhanyan National Science Laboratory (Yerevan Physics Institute) Foundation (ANSL), State Committee of Science and World Federation of Scientists (WFS), Armenia; Austrian Academy of Sciences, Austrian Science Fund (FWF): [M 2467-N36] and Nationalstiftung für Forschung, Technologie und Entwicklung, Austria; Ministry of Communications and High Technologies, National Nuclear Research Center, Azerbaijan; Conselho Nacional de Desenvolvimento Científico e Tecnológico (CNPq), Financiadora de Estudos e Projetos (Finep), Fundação de Amparo à Pesquisa do Estado de São Paulo (FAPESP) and Universidade Federal do Rio Grande do Sul (UFRGS), Brazil; Bulgarian Ministry of Education and Science, within the National Roadmap for Research Infrastructures 2020–2027 (object CERN), Bulgaria; Ministry of Education of China (MOEC), Ministry of Science & Technology of China (MSTC) and National Natural Science Foundation of China (NSFC), China; Ministry of Science and Education and Croatian Science Foundation, Croatia; Centro de Aplicaciones Tecnológicas y Desarrollo Nuclear (CEADEN), Cubaenergía, Cuba; Ministry of Education, Youth and Sports of the Czech Republic, Czech Republic; The Danish Council for Independent Research | Natural Sciences, the VILLUM FONDEN and Danish National Research Foundation (DNRF), Denmark; Helsinki Institute of Physics (HIP), Finland; Commissariat à l’Energie Atomique (CEA) and Institut National de Physique Nucléaire et de Physique des Particules (IN2P3) and Centre National de la Recherche Scientifique (CNRS), France; Bundesministerium für Bildung und Forschung (BMBF) and GSI Helmholtzzentrum für Schwerionenforschung GmbH, Germany; General Secretariat for Research and Technology, Ministry of Education, Research and Religions, Greece; National Research, Development and Innovation Office, Hungary; Department of Atomic Energy Government of India (DAE), Department of Science and Technology, Government of India (DST), University Grants Commission, Government of India (UGC) and Council of Scientific and Industrial Research (CSIR), India; National Research and Innovation Agency - BRIN, Indonesia; Istituto Nazionale di Fisica Nucleare (INFN), Italy; Japanese Ministry of Education, Culture, Sports, Science and Technology (MEXT) and Japan Society for the Promotion of Science (JSPS) KAKENHI, Japan; Consejo Nacional de Ciencia (CONACYT) y Tecnología, through Fondo de Cooperación Internacional en Ciencia y Tecnología (FONCICYT) and Dirección General de Asuntos del Personal Académico (DGAPA), Mexico; Nederlandse Organisatie voor Wetenschappelijk Onderzoek (NWO), Netherlands; The Research Council of Norway, Norway; Commission on Science and Technology for Sustainable Development in the South (COMSATS), Pakistan; Pontificia Universidad Católica del Perú, Peru; Ministry of Education and Science, National Science Centre and WUT ID-UB, Poland; Korea Institute of Science and Technology Information and National Research Foundation of Korea (NRF), Republic of Korea; Ministry of Education and Scientific Research, Institute of Atomic Physics, Ministry of Research and Innovation and Institute of Atomic Physics and University Politehnica of Bucharest, Romania; Ministry of Education, Science, Research and Sport of

the Slovak Republic, Slovakia; National Research Foundation of South Africa, South Africa; Swedish Research Council (VR) and Knut & Alice Wallenberg Foundation (KAW), Sweden; European Organization for Nuclear Research, Switzerland; Suranaree University of Technology (SUT), National Science and Technology Development Agency (NSTDA), Thailand Science Research and Innovation (TSRI) and National Science, Research and Innovation Fund (NSRF), Thailand; Turkish Energy, Nuclear and Mineral Research Agency (TENMAK), Turkey; National Academy of Sciences of Ukraine, Ukraine; Science and Technology Facilities Council (STFC), United Kingdom; National Science Foundation of the United States of America (NSF) and United States Department of Energy, Office of Nuclear Physics (DOE NP), United States of America. In addition, individual groups or members have received support from: Marie Skłodowska Curie, Strong 2020 - Horizon 2020, European Research Council (grant nos. 824093, 896850, 950692), European Union; Academy of Finland (Center of Excellence in Quark Matter) (grant nos. 346327, 346328), Finland; Programa de Apoyos para la Superación del Personal Académico, UNAM, Mexico.

References

- [1] D. E. Kharzeev, L. D. McLerran, and H. J. Warringa, “The Effects of topological charge change in heavy ion collisions: ‘Event by event P and CP violation’”, *Nucl. Phys. A* **803** (2008) 227, arXiv:0711.0950 [hep-ph].
- [2] M. Asakawa, A. Majumder, and B. Muller, “Electric Charge Separation in Strong Transient Magnetic Fields”, *Phys. Rev. C* **81** (2010) 064912, arXiv:1003.2436 [hep-ph].
- [3] K. Hattori and K. Itakura, “Vacuum birefringence in strong magnetic fields: (I) Photon polarization tensor with all the Landau levels”, *Annals Phys.* **330** (2013) 23, arXiv:1209.2663 [hep-ph].
- [4] V. Koch, S. Schlichting, V. Skokov, P. Sorensen, J. Thomas, S. Voloshin, G. Wang, and H.-U. Yee, “Status of the chiral magnetic effect and collisions of isobars”, *Chin. Phys. C* **41** (2017) 072001, arXiv:1608.00982 [nucl-th].
- [5] R. Battesti *et al.*, “High magnetic fields for fundamental physics”, *Phys. Rept.* **765-766** (2018) 1, arXiv:1803.07547 [physics.ins-det].
- [6] D. E. Kharzeev, J. Liao, S. A. Voloshin, and G. Wang, “Chiral magnetic and vortical effects in high-energy nuclear collisions—A status report”, *Prog. Part. Nucl. Phys.* **88** (2016) 1, arXiv:1511.04050 [hep-ph].
- [7] **STAR** Collaboration, B. I. Abelev *et al.*, “Azimuthal Charged-Particle Correlations and Possible Local Strong Parity Violation”, *Phys. Rev. Lett.* **103** (2009) 251601, arXiv:0909.1739 [nucl-ex].
- [8] **ALICE** Collaboration, B. Abelev *et al.*, “Charge separation relative to the reaction plane in Pb-Pb collisions at $\sqrt{s_{NN}} = 2.76$ TeV”, *Phys. Rev. Lett.* **110** (2013) 012301, arXiv:1207.0900 [nucl-ex].
- [9] **CMS** Collaboration, V. Khachatryan *et al.*, “Observation of charge-dependent azimuthal correlations in p -Pb collisions and its implication for the search for the chiral magnetic effect”, *Phys. Rev. Lett.* **118** (2017) 122301, arXiv:1610.00263 [nucl-ex].
- [10] G. Breit and J. A. Wheeler, “Collision of two light quanta”, *Phys. Rev.* **46** (1934) 1087.
- [11] **STAR** Collaboration, J. Adams *et al.*, “Production of e^+e^- pairs accompanied by nuclear dissociation in ultra-peripheral heavy ion collision”, *Phys. Rev. C* **70** (2004) 031902, arXiv:nucl-ex/0404012.

- [12] **STAR** Collaboration, J. Adam *et al.*, “Low- p_T e^+e^- pair production in Au+Au collisions at $\sqrt{s_{NN}} = 200$ GeV and U+U collisions at $\sqrt{s_{NN}} = 193$ GeV at STAR”, *Phys. Rev. Lett.* **121** (2018) 132301, arXiv:1806.02295 [hep-ex].
- [13] **ATLAS** Collaboration, M. Aaboud *et al.*, “Observation of centrality-dependent acoplanarity for muon pairs produced via two-photon scattering in Pb+Pb collisions at $\sqrt{s_{NN}} = 5.02$ TeV with the ATLAS detector”, *Phys. Rev. Lett.* **121** (2018) 212301, arXiv:1806.08708 [nucl-ex].
- [14] **ATLAS** Collaboration, “Measurement of muon pairs produced via $\gamma\gamma$ scattering in non-ultraperipheral Pb+Pb collisions at $\sqrt{s_{NN}} = 5.02$ TeV with the ATLAS detector”, *Phys. Rev. C* **107** (2023) 054907, arXiv:2206.12594 [nucl-ex].
- [15] E. Fermi, “On the theory of collisions between atoms and electrically charged particles”, *Nuovo Cim.* **2** (1925) 143, arXiv:hep-th/0205086.
- [16] C. F. von Weizsacker, “Radiation emitted in collisions of very fast electrons”, *Z. Phys.* **88** (1934) 612.
- [17] E. J. Williams, “Nature of the high-energy particles of penetrating radiation and status of ionization and radiation formulae”, *Phys. Rev.* **45** (1934) 729.
- [18] K. Hencken, D. Trautmann, and G. Baur, “Impact parameter dependence of the total probability for the electromagnetic electron - positron pair production in relativistic heavy ion collisions”, *Phys. Rev. A* **51** (1995) 1874, arXiv:nucl-th/9410014.
- [19] A. Alscher, K. Hencken, D. Trautmann, and G. Baur, “Multiple electromagnetic electron positron pair production in relativistic heavy ion collisions”, *Phys. Rev. A* **55** (1997) 396, arXiv:nucl-th/9606011.
- [20] M. Klusek-Gawenda, R. Rapp, W. Schäfer, and A. Szczurek, “Dilepton Radiation in Heavy-Ion Collisions at Small Transverse Momentum”, *Phys. Lett. B* **790** (2019) 339, arXiv:1809.07049 [nucl-th].
- [21] M. Klusek-Gawenda, W. Schäfer, and A. Szczurek, “Centrality dependence of dilepton production via $\gamma\gamma$ processes from Wigner distributions of photons in nuclei”, *Phys. Lett. B* **814** (2021) 136114, arXiv:2012.11973 [hep-ph].
- [22] **ALICE** Collaboration, E. Abbas *et al.*, “Charmonium and e^+e^- pair photoproduction at mid-rapidity in ultra-peripheral Pb-Pb collisions at $\sqrt{s_{NN}}=2.76$ TeV”, *Eur. Phys. J. C* **73** (2013) 2617, arXiv:1305.1467 [nucl-ex].
- [23] **CMS** Collaboration, A. M. Sirunyan *et al.*, “Evidence for light-by-light scattering and searches for axion-like particles in ultraperipheral PbPb collisions at $\sqrt{s_{NN}} = 5.02$ TeV”, *Phys. Lett. B* **797** (2019) 134826, arXiv:1810.04602 [hep-ex].
- [24] **ATLAS** Collaboration, G. Aad *et al.*, “Exclusive dimuon production in ultraperipheral Pb+Pb collisions at $\sqrt{s_{NN}} = 5.02$ TeV with ATLAS”, *Phys. Rev. C* **104** (2021) 024906, arXiv:2011.12211 [nucl-ex].
- [25] S. R. Klein, J. Nystrand, J. Seger, Y. Gorbunov, and J. Butterworth, “STARlight: A Monte Carlo simulation program for ultra-peripheral collisions of relativistic ions”, *Comput. Phys. Commun.* **212** (2017) 258, arXiv:1607.03838 [hep-ph].
- [26] **STAR** Collaboration, J. Adam *et al.*, “Measurement of e^+e^- Momentum and Angular Distributions from Linearly Polarized Photon Collisions”, *Phys. Rev. Lett.* **127** (2021) 052302, arXiv:1910.12400 [nucl-ex].

- [27] **CMS** Collaboration, A. M. Sirunyan *et al.*, “Observation of Forward Neutron Multiplicity Dependence of Dimuon Acoplanarity in Ultraperipheral Pb–Pb Collisions at $\sqrt{s_{NN}}=5.02$ TeV”, *Phys. Rev. Lett.* **127** (2021) 122001, arXiv:2011.05239 [hep-ex].
- [28] J. D. Brandenburg, W. Li, L. Ruan, Z. Tang, Z. Xu, S. Yang, and W. Zha, “Acoplanarity of QED pairs accompanied by nuclear dissociation in ultra-peripheral heavy ion collisions”, arXiv:2006.07365 [hep-ph].
- [29] W. Zha, J. D. Brandenburg, Z. Tang, and Z. Xu, “Initial transverse-momentum broadening of Breit-Wheeler process in relativistic heavy-ion collisions”, *Phys. Lett. B* **800** (2020) 135089, arXiv:1812.02820 [nucl-th].
- [30] M. Vidovic, M. Greiner, C. Best, and G. Soff, “Impact parameter dependence of the electromagnetic particle production in ultrarelativistic heavy ion collisions”, *Phys. Rev. C* **47** (1993) 2308.
- [31] K. Hencken, G. Baur, and D. Trautmann, “Production of QED pairs at small impact parameter in relativistic heavy ion collisions”, *Phys. Rev. C* **69** (2004) 054902, arXiv:nucl-th/0402061.
- [32] C. Li, J. Zhou, and Y.-J. Zhou, “Impact parameter dependence of the azimuthal asymmetry in lepton pair production in heavy ion collisions”, *Phys. Rev. D* **101** (2020) 034015, arXiv:1911.00237 [hep-ph].
- [33] S. Klein, A. H. Mueller, B.-W. Xiao, and F. Yuan, “Lepton pair production through two photon process in heavy ion collisions”, *Phys. Rev. D* **102** (2020) 094013, arXiv:2003.02947 [hep-ph].
- [34] R.-j. Wang, S. Pu, and Q. Wang, “Lepton pair production in ultraperipheral collisions”, *Phys. Rev. D* **104** (2021) 056011, arXiv:2106.05462 [hep-ph].
- [35] C. Li, J. Zhou, and Y.-J. Zhou, “Probing the linear polarization of photons in ultraperipheral heavy ion collisions”, *Phys. Lett. B* **795** (2019) 576, arXiv:1903.10084 [hep-ph].
- [36] W. Heisenberg and H. Euler, “Consequences of Dirac’s theory of positrons”, *Z. Phys.* **98** (1936) 714, arXiv:physics/0605038.
- [37] J. D. Brandenburg, W. Zha, and Z. Xu, “Mapping the electromagnetic fields of heavy-ion collisions with the Breit-Wheeler process”, *Eur. Phys. J. A* **57** (2021) 299, arXiv:2103.16623 [hep-ph].
- [38] G. Baur, “Coherent photon-photon interactions in very peripheral relativistic heavy ion collisions”, *Eur. Phys. J. D* **55** (2009) 265, arXiv:0810.1400 [nucl-th].
- [39] W. Zha and Z. Tang, “Discovery of higher order QED effect for the vacuum pair production”, *JHEP* **08** (2021) 083, arXiv:2103.04605 [hep-ph].
- [40] **ALICE** Collaboration, K. Aamodt *et al.*, “The ALICE experiment at the CERN LHC”, *JINST* **3** (2008) S08002.
- [41] **ALICE** Collaboration, B. B. Abelev *et al.*, “Performance of the ALICE Experiment at the CERN LHC”, *Int. J. Mod. Phys. A* **29** (2014) 1430044, arXiv:1402.4476 [nucl-ex].
- [42] **ALICE** Collaboration, K. Aamodt *et al.*, “Alignment of the ALICE Inner Tracking System with cosmic-ray tracks”, *JINST* **5** (2010) P03003, arXiv:1001.0502 [physics.ins-det].

- [43] J. Alme *et al.*, “The ALICE TPC, a large 3-dimensional tracking device with fast readout for ultra-high multiplicity events”, *Nucl. Instrum. Meth. A* **622** (2010) 316, arXiv:1001.1950 [physics.ins-det].
- [44] A. Akindinov *et al.*, “Performance of the ALICE Time-Of-Flight detector at the LHC”, *Eur. Phys. J. Plus* **128** (2013) 44.
- [45] ALICE Collaboration, E. Abbas *et al.*, “Performance of the ALICE VZERO system”, *JINST* **8** (2013) P10016.
- [46] R. Arnaldi *et al.*, “The Zero degree calorimeters for the ALICE experiment”, *Nucl. Instrum. Meth. A* **581** (2007) 397. [Erratum: *Nucl.Instrum.Meth.A* 604, 765 (2009)].
- [47] ALICE Collaboration, “Centrality determination in heavy ion collisions”, *ALICE-PUBLIC-2018-011* (2018) . <https://cds.cern.ch/record/2636623>.
- [48] ALICE Collaboration, S. Acharya *et al.*, “Dielectron production in proton-proton and proton-lead collisions at $\sqrt{s_{NN}} = 5.02$ TeV”, *Phys. Rev. C* **102** (2020) 055204, arXiv:2005.11995 [nucl-ex].
- [49] ALICE Collaboration, S. Acharya *et al.*, “Soft-dielectron excess in proton-proton collisions at $\sqrt{s} = 13$ TeV”, *Phys. Rev. Lett.* **127** (2021) 042302, arXiv:2005.14522 [nucl-ex].
- [50] ALICE Collaboration, S. Acharya *et al.*, “Dielectron and heavy-quark production in inelastic and high-multiplicity proton–proton collisions at $\sqrt{s_{NN}} = 13$ TeV”, *Phys. Lett. B* **788** (2019) 505, arXiv:1805.04407 [hep-ex].
- [51] PHENIX Collaboration, A. Adare *et al.*, “Detailed measurement of the $e^+ e^-$ pair continuum in p+p and Au+Au collisions at $\sqrt{s_{NN}} = 200$ GeV and implications for direct photon production”, *Phys. Rev. C* **81** (2010) 034911, arXiv:0912.0244 [nucl-ex].
- [52] ALICE Collaboration, S. Acharya *et al.*, “Measurement of dielectron production in central Pb-Pb collisions at $\sqrt{s_{NN}} = 2.76$ TeV”, *Phys. Rev. C* **99** (2019) 024002, arXiv:1807.00923 [nucl-ex].
- [53] R. Brun, F. Bruyant, M. Maire, A. C. McPherson, and P. Zancarini, *GEANT 3: user’s guide Geant 3.10, Geant 3.11; rev. version*. CERN, Geneva, 1987. <https://cds.cern.ch/record/1119728>.
- [54] X.-N. Wang and M. Gyulassy, “HIJING: A Monte Carlo model for multiple jet production in p p, p A and A A collisions”, *Phys. Rev. D* **44** (1991) 3501.
- [55] P. Golonka and Z. Was, “PHOTOS Monte Carlo: A Precision tool for QED corrections in Z and W decays”, *Eur. Phys. J. C* **45** (2006) 97, arXiv:hep-ph/0506026.
- [56] T. Sjostrand, S. Mrenna, and P. Z. Skands, “PYTHIA 6.4 Physics and Manual”, *JHEP* **05** (2006) 026, arXiv:hep-ph/0603175.
- [57] P. Z. Skands, “Tuning Monte Carlo Generators: The Perugia Tunes”, *Phys. Rev. D* **82** (2010) 074018, arXiv:1005.3457 [hep-ph].
- [58] R. J. Barlow and C. Beeston, “Fitting using finite Monte Carlo samples”, *Comput. Phys. Commun.* **77** (1993) 219.
- [59] ALICE Collaboration, “Momentum transformation matrix for dielectron simulations in Pb-Pb collisions at $\sqrt{s_{NN}} = 2.76$ TeV”, *ALICE-PUBLIC-2017-011* (2017) . <https://cds.cern.ch/record/2289779>.

- [60] **ALICE** Collaboration, S. Acharya *et al.*, “Dielectron production in proton-proton collisions at $\sqrt{s} = 7$ TeV”, *JHEP* **09** (2018) 064, arXiv:1805.04391 [hep-ex].
- [61] **WA80** Collaboration, R. Albrecht *et al.*, “Production of eta mesons in 200-A/GeV S + S and S + Au reactions”, *Phys. Lett. B* **361** (1995) 14, arXiv:hep-ex/9507009.
- [62] P. K. Khandai, P. Shukla, and V. Singh, “Meson spectra and m_T scaling in $p + p$, $d + Au$, and $Au + Au$ collisions at $\sqrt{s_{NN}} = 200$ GeV”, *Phys. Rev. C* **84** (2011) 054904, arXiv:1110.3929 [hep-ph].
- [63] L. Altenkämper, F. Bock, C. Loizides, and N. Schmidt, “Applicability of transverse mass scaling in hadronic collisions at energies available at the CERN Large Hadron Collider”, *Phys. Rev. C* **96** (2017) 064907, arXiv:1710.01933 [hep-ph].
- [64] **ALICE** Collaboration, S. Acharya *et al.*, “Production of charged pions, kaons, and (anti-)protons in Pb-Pb and inelastic pp collisions at $\sqrt{s_{NN}} = 5.02$ TeV”, *Phys. Rev. C* **101** (2020) 044907, arXiv:1910.07678 [nucl-ex].
- [65] A. A. Bylinkin and A. A. Rostovtsev, “Parametrization of the shape of hadron-production spectra in high-energy particle interactions”, *Phys. Atom. Nucl.* **75** (2012) 999.
- [66] A. Bylinkin, N. S. Chernyavskaya, and A. A. Rostovtsev, “Predictions on the transverse momentum spectra for charged particle production at LHC-energies from a two component model”, *Eur. Phys. J. C* **75** (2015) 166, arXiv:1501.05235 [hep-ph].
- [67] K. Reygers, A. Schmah, A. Berdnikova, and X. Sun, “Blast-wave description of Υ elliptic flow at energies available at the CERN Large Hadron Collider”, *Phys. Rev. C* **101** (2020) 064905, arXiv:1910.14618 [hep-ph].
- [68] G. Agakichiev *et al.*, “Neutral meson production in p–Be and p–Au collisions at 450 GeV beam energy”, *Eur. Phys. J. C* **4** (1998) 249.
- [69] **ALICE** Collaboration, S. Acharya *et al.*, “Production of ω mesons in pp collisions at $\sqrt{s} = 7$ TeV”, *Eur. Phys. J. C* **80** (2020) 1130, arXiv:2007.02208 [nucl-ex].
- [70] **PHENIX** Collaboration, A. Adare *et al.*, “Production of ω mesons in $p + p$, $d + Au$, $Cu + Cu$, and $Au + Au$ collisions at $\sqrt{s_{NN}} = 200$ GeV”, *Phys. Rev. C* **84** (2011) 044902, arXiv:1105.3467 [nucl-ex].
- [71] **ALICE** Collaboration, S. Acharya *et al.*, “Evidence of rescattering effect in Pb-Pb collisions at the LHC through production of $K^*(892)^0$ and $\phi(1020)$ mesons”, *Phys. Lett. B* **802** (2020) 135225, arXiv:1910.14419 [nucl-ex].
- [72] P. Nason, “A New method for combining NLO QCD with shower Monte Carlo algorithms”, *JHEP* **11** (2004) 040, arXiv:hep-ph/0409146 [hep-ph].
- [73] S. Frixione, P. Nason, and G. Ridolfi, “A Positive-weight next-to-leading-order Monte Carlo for heavy flavour hadroproduction”, *JHEP* **09** (2007) 126.
- [74] S. Frixione, P. Nason, and C. Oleari, “Matching NLO QCD computations with Parton Shower simulations: the POWHEG method”, *JHEP* **11** (2007) 070.
- [75] S. Alioli, P. Nason, C. Oleari, and E. Re, “A general framework for implementing NLO calculations in shower Monte Carlo programs: the POWHEG BOX”, *JHEP* **06** (2010) 043, arXiv:1002.2581 [hep-ph].

- [76] G. J. Feldman and R. D. Cousins, “A Unified approach to the classical statistical analysis of small signals”, *Phys. Rev. D* **57** (1998) 3873, arXiv:physics/9711021.
- [77] R. Rapp and J. Wambach, “Low mass dileptons at the CERN SPS: Evidence for chiral restoration?”, *Eur. Phys. J. A* **6** (1999) 415, arXiv:hep-ph/9907502.
- [78] H. van Hees and R. Rapp, “Dilepton Radiation at the CERN Super Proton Synchrotron”, *Nucl. Phys. A* **806** (2008) 339, arXiv:0711.3444 [hep-ph].
- [79] R. Rapp, “Dilepton Spectroscopy of QCD Matter at Collider Energies”, *Adv. High Energy Phys.* **2013** (2013) 148253, arXiv:1304.2309 [hep-ph].
- [80] NA60 Collaboration, R. Arnaldi *et al.*, “First measurement of the rho spectral function in high-energy nuclear collisions”, *Phys. Rev. Lett.* **96** (2006) 162302, arXiv:nuc1-ex/0605007.
- [81] CERES Collaboration, D. Adamova *et al.*, “Modification of the rho-meson detected by low-mass electron-positron pairs in central Pb-Au collisions at 158-A-GeV/c”, *Phys. Lett. B* **666** (2008) 425, arXiv:nuc1-ex/0611022.
- [82] STAR Collaboration, L. Adamczyk *et al.*, “Dielectron mass spectra from Au+Au Collisions at $\sqrt{s_{NN}} = 200$ GeV”, *Phys. Rev. Lett.* **113** (2014) 022301, arXiv:1312.7397 [hep-ex]. [Addendum: *Phys.Rev.Lett.* 113, 049903 (2014)].
- [83] PHENIX Collaboration, A. Adare *et al.*, “Dielectron production in Au+Au collisions at $\sqrt{s_{NN}}=200$ GeV”, *Phys. Rev. C* **93** (2016) 014904, arXiv:1509.04667 [nuc1-ex].
- [84] M. Klusek-Gawenda and A. Szczurek, “Exclusive muon-pair productions in ultrarelativistic heavy-ion collisions – realistic nucleus charge form factor and differential distributions”, *Phys. Rev. C* **82** (2010) 014904, arXiv:1004.5521 [nuc1-th].
- [85] S. R. Klein, “Two-photon production of dilepton pairs in peripheral heavy ion collisions”, *Phys. Rev. C* **97** (2018) 054903, arXiv:1801.04320 [nuc1-th].
- [86] ALICE Collaboration, “Photoproduction of low- p_T J/ψ from peripheral to central Pb–Pb collisions at 5.02 TeV”, arXiv:2204.10684 [nuc1-ex].
- [87] M. B. Gay Ducati and S. Martins, “Heavy meson photoproduction in peripheral AA collisions”, *Phys. Rev. D* **97** (2018) 116013, arXiv:1804.09836 [hep-ph].
- [88] ALICE Collaboration, “Upgrade of the Inner Tracking System Conceptual Design Report. Conceptual Design Report for the Upgrade of the ALICE ITS”, *CERN-LHCC-2012-013* (2012) . <https://cds.cern.ch/record/1475244>.
- [89] ALICE Collaboration, “Upgrade of the ALICE Time Projection Chamber”, *CERN-LHCC-2013-020* (2013) . <https://cds.cern.ch/record/1622286>.
- [90] ALICE Collaboration, “Addendum to the Technical Design Report for the Upgrade of the ALICE Time Projection Chamber”, *CERN-LHCC-2015-002* (2015) . <https://cds.cern.ch/record/1984329>.

A The ALICE Collaboration

S. Acharya ^{124,131}, D. Adamová ⁸⁶, A. Adler⁶⁹, G. Aglieri Rinella ³², M. Agnello ²⁹, N. Agrawal ⁵⁰, Z. Ahammed ¹³¹, S. Ahmad ¹⁵, S.U. Ahn ⁷⁰, I. Ahuja ³⁷, A. Akindinov ¹³⁹, M. Al-Turany ⁹⁸, D. Aleksandrov ¹³⁹, B. Alessandro ⁵⁵, H.M. Alfanda ⁶, R. Alfaro Molina ⁶⁶, B. Ali ¹⁵, Y. Ali¹³, A. Alici ²⁵, N. Alizadehvandchali ¹¹³, A. Alkin ³², J. Alme ²⁰, G. Alocco ⁵¹, T. Alt ⁶³, I. Altsybeev ¹³⁹, M.N. Anaam ⁶, C. Andrei ⁴⁵, A. Andronic ¹³⁴, V. Anguelov ⁹⁵, F. Antinori ⁵³, P. Antonioli ⁵⁰, C. Anuj ¹⁵, N. Apadula ⁷⁴, L. Aphecetche ¹⁰³, H. Appelshäuser ⁶³, S. Arcelli ²⁵, R. Arnaldi ⁵⁵, I.C. Arsene ¹⁹, M. Arslanok ¹³⁶, A. Augustinus ³², R. Averbeck ⁹⁸, S. Aziz ⁷², M.D. Azmi ¹⁵, A. Badalà ⁵², Y.W. Baek ⁴⁰, X. Bai ⁹⁸, R. Bailhache ⁶³, Y. Bailung ⁴⁷, R. Bala ⁹¹, A. Balbino ²⁹, A. Baldisseri ¹²⁷, B. Balis ², D. Banerjee ⁴, Z. Banoo ⁹¹, R. Barbera

²⁶, L. Barioglio ⁹⁶, M. Barlou⁷⁸, G.G. Barnaföldi ¹³⁵, L.S. Barnby ⁸⁵, V. Barret ¹²⁴, L. Barreto ¹⁰⁹, C. Bartels ¹¹⁶, K. Barth ³², E. Bartsch ⁶³, F. Baruffaldi ²⁷, N. Bastid ¹²⁴, S. Basu ⁷⁵, G. Batigne ¹⁰³, D. Battistini ⁹⁶, B. Batyunya ¹⁴⁰, D. Bauri⁴⁶, J.L. Bazo Alba ¹⁰¹, I.G. Bearden ⁸³, C. Beattie ¹³⁶, P. Becht ⁹⁸, D. Behera ⁴⁷, I. Belikov ¹²⁶, A.D.C. Bell Hechavarria ¹³⁴, F. Bellini ²⁵, R. Bellwied ¹¹³, S. Belokurova ¹³⁹, V. Belyaev ¹³⁹, G. Bencedi ^{135,64}, S. Beole ²⁴, A. Bercuci ⁴⁵, Y. Berdnikov ¹³⁹, A. Berdnikova ⁹⁵, L. Bergmann ⁹⁵, M.G. Besoiu ⁶², L. Betev ³², P.P. Bhaduri ¹³¹, A. Bhasin ⁹¹, I.R. Bhat⁹¹, M.A. Bhat ⁴, B. Bhattacharjee ⁴¹, L. Bianchi ²⁴, N. Bianchi ⁴⁸, J. Bielčák ³⁵, J. Bielčiková ⁸⁶, J. Biernat ¹⁰⁶, A. Bilandzic ⁹⁶, G. Biro ¹³⁵, S. Biswas ⁴, J.T. Blair ¹⁰⁷, D. Blau ¹³⁹, M.B. Blidaru ⁹⁸, N. Bluhme³⁸, C. Blume ⁶³, G. Boca ^{21,54}, F. Bock ⁸⁷, T. Bodova ²⁰, A.
Bogdanov¹³⁹, S. Boi ²², J. Bok ⁵⁷, L. Boldizsár ¹³⁵, A. Bolozdynya ¹³⁹, M. Bombara ³⁷, P.M. Bond ³², G. Bonomi ^{130,54}, H. Borel ¹²⁷, A. Borissov ¹³⁹, H. Bossi ¹³⁶, E. Botta ²⁴, L. Bratrud ⁶³, P. Braun-Munzinger ⁹⁸, M. Bregant ¹⁰⁹, M. Broz ³⁵, G.E. Bruno ^{97,31}, M.D. Buckland ¹¹⁶, D. Budnikov ¹³⁹, H. Buesching ⁶³, S. Bufalino ²⁹, O. Bugnon¹⁰³, P. Buhler ¹⁰², Z. Buthelezi ^{67,120}, J.B. Butt¹³, A. Bylinkin ¹¹⁵, S.A. Bysiak¹⁰⁶, M. Cai ^{27,6}, H. Caines ¹³⁶, A. Caliva ⁹⁸, E. Calvo Villar ¹⁰¹, J.M.M. Camacho ¹⁰⁸, R.S. Camacho⁴⁴, P. Camerini ²³, F.D.M. Canedo ¹⁰⁹, M. Carabas ¹²³, F. Carnesecchi ³², R. Caron ^{125,127}, J. Castillo Castellanos ¹²⁷, F. Catalano ²⁹, C. Ceballos Sanchez ¹⁴⁰, I. Chakaberia ⁷⁴, P. Chakraborty ⁴⁶, S. Chandra ¹³¹, S. Chapeland ³², M. Chartier ¹¹⁶, S. Chattopadhyay ¹³¹, S. Chattopadhyay ⁹⁹, T.G. Chavez ⁴⁴, T. Cheng ⁶, C. Cheshkov ¹²⁵, B. Cheynis ¹²⁵, V. Chibante Barroso ³², D.D. Chinellato ¹¹⁰, E.S. Chizzali ^{11,96}, J. Cho ⁵⁷, S. Cho

⁵⁷, P. Chochula ³², P. Christakoglou ⁸⁴, C.H. Christensen ⁸³, P. Christiansen ⁷⁵, T. Chujo ¹²², M. Ciacco ²⁹, C. Cicalo ⁵¹, L. Cifarelli ²⁵, F. Cindolo ⁵⁰, M.R. Ciupek ⁹⁸, G. Clai^{III,50}, F. Colamaria ⁴⁹, J.S. Colburn¹⁰⁰, D. Colella ^{97,31}, A. Collu⁷⁴, M. Colocci ³², M. Concas ^{IV,55}, G. Conesa Balbastre ⁷³, Z. Conesa del Valle ⁷², G. Contin ²³, J.G. Contreras ³⁵, M.L. Coquet ¹²⁷, T.M. Cormier^{I,87}, P. Cortese ^{129,55}, M.R. Cosentino ¹¹¹, F. Costa ³², S. Costanza ^{21,54}, P. Crochet ¹²⁴, R. Cruz-Torres ⁷⁴, E. Cuautele⁶⁴, P. Cui ⁶, L. Cunqueiro⁸⁷, A. Dainese ⁵³, M.C. Danisch ⁹⁵, A. Danu ⁶², P. Das ⁸⁰, P. Das ⁴, S. Das ⁴, S. Dash ⁴⁶, A. De Caro ²⁸, G. de Cataldo ⁴⁹, L. De Cilladi ²⁴, J. de Cuveland³⁸, A. De Falco ²², D. De Gruttola ²⁸, N. De Marco ⁵⁵, C. De Martin ²³, S. De Pasquale ²⁸, S. Deb ⁴⁷, H.F. Degenhardt¹⁰⁹, K.R. Deja ¹³², R. Del Grande ⁹⁶, L. Dello Stritto ²⁸, W. Deng ⁶, P. Dhankher ¹⁸, D. Di Bari ³¹, A. Di Mauro ³², R.A. Diaz ^{140,7}, T. Dietel ¹¹², Y. Ding

^{125,6}, R. Divià ³², D.U. Dixit ¹⁸, Ø. Djuvland²⁰, U. Dmitrieva ¹³⁹, A. Dobrin ⁶², B. Dönigus ⁶³, A.K. Dubey ¹³¹, J.M. Dubinski¹³², A. Dubla ⁹⁸, S. Dudi ⁹⁰, P. Dupieux ¹²⁴, M. Durkac¹⁰⁵, N. Dzalaiova¹², T.M. Eder ¹³⁴, R.J. Ehlers ⁸⁷, V.N. Eikeland²⁰, F. Eisenhut ⁶³, D. Elia ⁴⁹, B. Erasmus ¹⁰³, F. Ercolessi ²⁵, F. Erhardt ⁸⁹, M.R. Ersdal²⁰, B. Espagnon ⁷², G. Eulisse ³², D. Evans ¹⁰⁰, S. Evdokimov ¹³⁹, L. Fabbietti ⁹⁶, M. Faggin ²⁷, J. Faivre ⁷³, F. Fan ⁶, W. Fan ⁷⁴, A. Fantoni ⁴⁸, M. Fasel ⁸⁷, P. Fedchio²⁹, A. Feliciello ⁵⁵, G. Feofilov ¹³⁹, A. Fernández Téllez ⁴⁴, M.B. Ferrer ³², A. Ferrero ¹²⁷, A. Ferretti ²⁴, V.J.G. Feuillard ⁹⁵, J. Figiel ¹⁰⁶, V. Filova³⁵, D. Finogeev ¹³⁹, F.M. Fionda ⁵¹, G. Fiorenza⁹⁷, F. Flor ¹¹³, A.N. Flores ¹⁰⁷, S. Foertsch ⁶⁷, I. Fokin ⁹⁵, S. Fokin ¹³⁹, E. Fragiaco ⁵⁶, E. Frajna ¹³⁵, U. Fuchs ³², N. Funicello ²⁸, C. Furget ⁷³, A. Furs ¹³⁹, J.J. Gaardhøje ⁸³, M. Gagliardi ²⁴, A.M. Gago ¹⁰¹, A. Gal¹²⁶, C.D. Galvan

¹⁰⁸, P. Ganoti ⁷⁸, C. Garabatos ⁹⁸, J.R.A. Garcia ⁴⁴, E. Garcia-Solis ⁹, K. Garg ¹⁰³, C. Gargiulo ³², A. Garibli⁸¹, K. Garner¹³⁴, E.F. Gauger ¹⁰⁷, A. Gautam ¹¹⁵, M.B. Gay Ducati ⁶⁵, M. Germain ¹⁰³, S.K. Ghosh⁴, M. Giacalone ²⁵, P. Gianotti ⁴⁸, P. Giubellino ^{98,55}, P. Giubilato ²⁷, A.M.C. Glaenger ¹²⁷, P. Glässel ⁹⁵, E. Glimos¹¹⁹, D.J.Q. Goh⁷⁶, V. Gonzalez ¹³³, L.H. González-Trueba ⁶⁶, S. Gorbunov³⁸, M. Gorgon ², L. Görlich ¹⁰⁶, S. Gotovac³³, V. Grabski ⁶⁶, L.K. Graczykowski ¹³², E. Grecka ⁸⁶, L. Greiner ⁷⁴, A. Grelli ⁵⁸, C. Grigoras ³², V. Grigoriev ¹³⁹, S. Grigoryan ^{140,1}, F. Grosa ³², J.F. Grosse-Oetringhaus ³², R. Grosso ⁹⁸, D. Grund

S.P. Guzman⁴⁴, L. Gyulai¹³⁵, M.K. Habib⁹⁸, C. Hadjidakis⁷², H. Hamagaki⁷⁶, M. Hamid⁶, Y. Han¹³⁷, R. Hannigan¹⁰⁷, M.R. Haque¹³², A. Harlenderova⁹⁸, J.W. Harris¹³⁶, A. Harton⁹, J.A. Hasenbichler³², H. Hassan⁸⁷, D. Hatzifotiadou⁵⁰, P. Hauer⁴², L.B. Havener¹³⁶, S.T. Heckel⁹⁶, E. Hellbär⁹⁸, H. Helstrup³⁴, T. Herman³⁵, G. Herrera Corral⁸, F. Herrmann¹³⁴, K.F. Hetland³⁴, B. Heybeck⁶³, H. Hillemanns³², C. Hills¹¹⁶, B. Hippolyte¹²⁶, B. Hofman⁵⁸, B. Hohlweger⁸⁴, J. Honeremann¹³⁴, G.H. Hong¹³⁷, D. Horak³⁵, A. Horzyk², R. Hosokawa¹⁴, Y. Hou⁶, P. Hristov³², C. Hughes¹¹⁹, P. Huhn⁶³, L.M. Huhta¹¹⁴, C.V. Hulse⁷², T.J. Humanic⁸⁸, H. Hushnud⁹⁹, A. Hutson¹¹³, D. Hutter³⁸, J.P. Iddon¹¹⁶, R. Ilkaev¹³⁹, H. Ilyas¹³, M. Inaba¹²², G.M. Innocenti³², M. Ippolitov¹³⁹, A. Isakov⁸⁶, T. Isidori¹¹⁵, M.S. Islam⁹⁹, M. Ivanov⁹⁸, V. Ivanov¹³⁹, V. Izucheev¹³⁹, M. Jablonski², B. Jacak⁷⁴, N. Jacazio³², P.M. Jacobs⁷⁴, S. Jadlovská¹⁰⁵, J. Jadlovsky¹⁰⁵, L. Jaffe³⁸, C. Jahnke¹¹⁰, M.A. Janik¹³², T. Janson⁶⁹, M. Jercic⁸⁹, O. Jevons¹⁰⁰, A.A.P. Jimenez⁶⁴, F. Jonas^{87,134}, P.G. Jones¹⁰⁰, J.M. Jowett^{32,98}, J. Jung⁶³, M. Jung⁶³, A. Junique³², A. Jusko¹⁰⁰, M.J. Kabus^{32,132}, J. Kaewjai¹⁰⁴, P. Kalinak⁵⁹, A.S. Kalteyer⁹⁸, A. Kalweit³², V. Kaplin¹³⁹, A. Karasu Uysal⁷¹, D. Karatovic⁸⁹, O. Karavichev¹³⁹, T. Karavicheva¹³⁹, P. Karczmarczyk¹³², E. Karpechev¹³⁹, V. Kashyap⁸⁰, A. Kazantsev¹³⁹, U. Keschull⁶⁹, R. Keidel¹³⁸, D.L.D. Keijdener⁵⁸, M. Keil³², B. Ketzer⁴², A.M. Khan⁶, S. Khan¹⁵, A. Khanzadeev¹³⁹, Y. Kharlov¹³⁹, A. Khatun¹⁵, A. Khuntia¹⁰⁶, B. Kileng³⁴, B. Kim¹⁶, C. Kim¹⁶, D.J. Kim¹¹⁴, E.J. Kim⁶⁸, J. Kim¹³⁷, J.S. Kim⁴⁰, J. Kim⁹⁵, J. Kim⁶⁸, M. Kim⁹⁵, S. Kim¹⁷, T. Kim¹³⁷, S. Kirsch⁶³, I. Kisel³⁸, S. Kiselev¹³⁹, A. Kisiel¹³², J.P. Kitowski², J.L. Klay⁵, J. Klein³², S. Klein⁷⁴, C. Klein-Bösing¹³⁴, M. Kleiner⁶³, T. Klemenz⁹⁶, A. Kluge³², A.G. Knospe¹¹³, C. Kobdaj¹⁰⁴, T. Kollegger⁹⁸, A. Kondratyev¹⁴⁰, N. Kondratyeva¹³⁹, E. Kondratyuk¹³⁹, J. Konig⁶³, S.A. Konigstorfer⁹⁶, P.J. Konopka³², G. Kornakov¹³², S.D. Koryciak², A. Kotliarov⁸⁶, O. Kovalenko⁷⁹, V. Kovalenko¹³⁹, M. Kowalski¹⁰⁶, I. Králík⁵⁹, A. Kravčáková³⁷, L. Kreis⁹⁸, M. Krivda^{100,59}, F. Krizek⁸⁶, K. Krizkova Gajdosova³⁵, M. Kroesen⁹⁵, M. Krüger⁶³, D.M. Krupova³⁵, E. Kryshen¹³⁹, M. Krzewicki³⁸, V. Kučera³², C. Kuhn¹²⁶, P.G. Kuijer⁸⁴, T. Kumaoka¹²², D. Kumar¹³¹, L. Kumar⁹⁰, N. Kumar⁹⁰, S. Kundu³², P. Kurashvili⁷⁹, A. Kurepin¹³⁹, A.B. Kurepin¹³⁹, S. Kushpil⁸⁶, J. Kvapil¹⁰⁰, M.J. Kweon⁵⁷, J.Y. Kwon⁵⁷, Y. Kwon¹³⁷, S.L. La Pointe³⁸, P. La Rocca²⁶, Y.S. Lai⁷⁴, A. Lakrathok¹⁰⁴, M. Lamanna³², R. Langoy¹¹⁸, P. Larionov⁴⁸, E. Laudi³², L. Lautner^{32,96}, R. Lavicka¹⁰², T. Lazareva¹³⁹, R. Lea^{130,54}, J. Leibrach³⁸, R.C. Lemmon⁸⁵, I. León Monzón¹⁰⁸, M.M. Lesch⁹⁶, E.D. Lesser¹⁸, M. Lettrich⁹⁶, P. Lévai¹³⁵, X. Li¹⁰, X.L. Li⁶, J. Lien¹¹⁸, R. Lietava¹⁰⁰, B. Lim¹⁶, S.H. Lim¹⁶, V. Lindenstruth³⁸, A. Lindner⁴⁵, C. Lippmann⁹⁸, A. Liu¹⁸, D.H. Liu⁶, J. Liu¹¹⁶, I.M. Lofnes²⁰, V. Loginov¹³⁹, C. Loizides⁸⁷, P. Loncar³³, J.A. Lopez⁹⁵, X. Lopez¹²⁴, E. López Torres⁷, P. Lu^{98,117}, J.R. Luhder¹³⁴, M. Lunardon²⁷, G. Luparello⁵⁶, Y.G. Ma³⁹, A. Maevskaya¹³⁹, M. Mager³², T. Mahmoud⁴², A. Maire¹²⁶, M. Malaev¹³⁹, N.M. Malik⁹¹, Q.W. Malik¹⁹, S.K. Malik⁹¹, L. Malinina^{VII,140}, D. Mal'Kevich¹³⁹, D. Mallick⁸⁰, N. Mallick⁴⁷, G. Mandaglio^{30,52}, V. Manko¹³⁹, F. Manso¹²⁴, V. Manzari⁴⁹, Y. Mao⁶, G.V. Margagliotti²³, A. Margotti⁵⁰, A. Marín⁹⁸, C. Markert¹⁰⁷, M. Marquard⁶³, N.A. Martin⁹⁵, P. Martinengo³², J.L. Martinez¹¹³, M.I. Martínez⁴⁴, G. Martínez García¹⁰³, S. Masciocchi⁹⁸, M. Maserà²⁴, A. Masoni⁵¹, L. Massacrier⁷², A. Mastroserio^{128,49}, A.M. Mathis⁹⁶, O. Matonoha⁷⁵, P.F.T. Matuoka¹⁰⁹, A. Matyja¹⁰⁶, C. Mayer¹⁰⁶, A.L. Mazuecos³², F. Mazzaschi²⁴, M. Mazzilli³², J.E. Mdhuli¹²⁰, A.F. Mechler⁶³, Y. Melikyan¹³⁹, A. Menchaca-Rocha⁶⁶, E. Meninno^{102,28}, A.S. Menon¹¹³, M. Meres¹², S. Mhlanga^{112,67}, Y. Miake¹²², L. Micheletti⁵⁵, L.C. Migliorin¹²⁵, D.L. Mihaylov⁹⁶, K. Mikhaylov^{140,139}, A.N. Mishra¹³⁵, D. Miśkowiec⁹⁸, A. Modak⁴, A.P. Mohanty⁵⁸, B. Mohanty⁸⁰, M. Mohisin Khan^{V,15}, M.A. Molander⁴³, Z. Moravcova⁸³, C. Mordasini⁹⁶, D.A. Moreira De Godoy¹³⁴, I. Morozov¹³⁹, A. Morsch³², T. Mrnjavac³², V. Muccifora⁴⁸, E. Mudnic³³, S. Muhuri¹³¹, J.D. Mulligan⁷⁴, A. Mulliri²², M.G. Munhoz¹⁰⁹, R.H. Munzer⁶³, H. Murakami¹²¹, S. Murray¹¹², L. Musa³², J. Musinsky⁵⁹, J.W. Myrcha¹³², B. Naik¹²⁰, R. Nair⁷⁹, B.K. Nandi⁴⁶, R. Nania⁵⁰, E. Nappi⁴⁹, A.F. Nassirpour⁷⁵, A. Nath⁹⁵, C. Nattrass¹¹⁹, A. Neagu¹⁹, A. Negru¹²³, L. Nellen⁶⁴, S.V. Nesbo³⁴, G. Neskovic³⁸, D. Nesterov¹³⁹, B.S. Nielsen⁸³, E.G. Nielsen⁸³, S. Nikolaev¹³⁹, S. Nikulin¹³⁹, V. Nikulin¹³⁹, F. Noferini⁵⁰, S. Noh¹¹, P. Nomokonov¹⁴⁰, J. Norman¹¹⁶, N. Novitzky¹²², P. Nowakowski¹³², A. Nyanin¹³⁹, J. Nystrand²⁰, M. Ogino⁷⁶, A. Ohlson⁷⁵, V.A. Okorokov¹³⁹, J. Olińczak¹³², A.C. Oliveira Da Silva¹¹⁹, M.H. Oliver¹³⁶, A. Onnerstad¹¹⁴, C. Oppedisano⁵⁵, A. Ortiz Velasquez⁶⁴, A. Oskarsson⁷⁵, J. Otwinowski¹⁰⁶, M. Oya⁹³, K. Oyama⁷⁶, Y. Pachmayer⁹⁵, S. Padhan⁴⁶, D. Pagano^{130,54}, G. Paic⁶⁴, A. Palasciano⁴⁹, S. Panebianco¹²⁷, J. Park⁵⁷, J.E. Parkkila^{32,114}, S.P. Pathak¹¹³, R.N. Patra⁹¹, B. Paul²², H. Pei⁶, T. Peitzmann⁵⁸, X. Peng⁶, L.G. Pereira⁶⁵, H. Pereira Da Costa¹²⁷, D. Peresunko¹³⁹, G.M. Perez⁷, S. Perrin¹²⁷, Y. Pestov¹³⁹,

V. Petráček³⁵, V. Petrov¹³⁹, M. Petrovici⁴⁵, R.P. Pezzi^{103,65}, S. Piano⁵⁶, M. Pikna¹², P. Pillot¹⁰³, O. Pinazza^{50,32}, L. Pinsky¹¹³, C. Pinto^{96,26}, S. Pisano⁴⁸, M. Płoskoń⁷⁴, M. Planinic⁸⁹, F. Pliquett⁶³, M.G. Poghosyan⁸⁷, S. Politano²⁹, N. Poljak⁸⁹, A. Pop⁴⁵, S. Porteboeuf-Houssais¹²⁴, J. Porter⁷⁴, V. Pozdniakov¹⁴⁰, S.K. Prasad⁴, S. Prasad⁴⁷, R. Preghenella⁵⁰, F. Prino⁵⁵, C.A. Pruneau¹³³, I. Pshenichnov¹³⁹, M. Puccio³², S. Qiu⁸⁴, L. Quaglia²⁴, R.E. Quishpe¹¹³, S. Ragoni¹⁰⁰, A. Rakotozafindrabe¹²⁷, L. Ramello^{129,55}, F. Rami¹²⁶, S.A.R. Ramirez⁴⁴, T.A. Rancien⁷³, R. Raniwala⁹², S. Raniwala⁹², S.S. Räsänen⁴³, R. Rath⁴⁷, I. Ravasenga⁸⁴, K.F. Read^{87,119}, A.R. Redelbach³⁸, K. Redlich^{VI,79}, A. Rehman²⁰, P. Reichelt⁶³, F. Reidt³², H.A. Reme-Ness³⁴, Z. Rescakova³⁷, K. Reygers⁹⁵, A. Riabov¹³⁹, V. Riabov¹³⁹, R. Ricci²⁸, T. Richert⁷⁵, M. Richter¹⁹, W. Riegler³², F. Riggi²⁶, C. Ristea⁶², M. Rodríguez Cahuantzi⁴⁴, K. Røed¹⁹, R. Rogalev¹³⁹, E. Rogochaya¹⁴⁰, T.S. Rogoschinski⁶³, D. Rohr³², D. Röhrich²⁰, P.F. Rojas⁴⁴, S. Rojas Torres³⁵, P.S. Rokita¹³², F. Ronchetti⁴⁸, A. Rosano^{30,52}, E.D. Rosas⁶⁴, A. Rossi⁵³, A. Roy⁴⁷, P. Roy⁹⁹, S. Roy⁴⁶, N. Rubini²⁵, O.V. Rueda⁷⁵, D. Ruggiano¹³², R. Rui²³, B. Rumyantsev¹⁴⁰, P.G. Russek², R. Russo⁸⁴, A. Rustamov⁸¹, E. Ryabinkin¹³⁹, Y. Ryabov¹³⁹, A. Rybicki¹⁰⁶, H. Rytkonen¹¹⁴, W. Rzesza¹³², O.A.M. Saarimäki⁴³, R. Sadek¹⁰³, S. Sadovsky¹³⁹, J. Saetre²⁰, K. Šafařík³⁵, S.K. Saha¹³¹, S. Saha⁸⁰, B. Sahoo⁴⁶, P. Sahoo⁴⁶, R. Sahoo⁴⁷, S. Sahoo⁶⁰, D. Sahu⁴⁷, P.K. Sahu⁶⁰, J. Saini¹³¹, K. Sajdakova³⁷, S. Sakai¹²², M.P. Salvan⁹⁸, S. Sambyal⁹¹, T.B. Saramela¹⁰⁹, D. Sarkar¹³³, N. Sarkar¹³¹, P. Sarma⁴¹, V. Sarritzu²², V.M. Sarti⁹⁶, M.H.P. Sas¹³⁶, J. Schambach⁸⁷, H.S. Scheid⁶³, C. Schiaua⁴⁵, R. Schicker⁹⁵, A. Schmah⁹⁵, C. Schmidt⁹⁸, H.R. Schmidt⁹⁴, M.O. Schmidt³², M. Schmidt⁹⁴, N.V. Schmidt^{87,63}, A.R. Schmier¹¹⁹, R. Schotter¹²⁶, J. Schukraft³², K. Schwarz⁹⁸, K. Schweda⁹⁸, G. Scioli²⁵, E. Scomparin⁵⁵, J.E. Seger¹⁴, Y. Sekiguchi¹²¹, D. Sekihata¹²¹, I. Selyuzhenkov^{98,139}, S. Senyukov¹²⁶, J.J. Seo⁵⁷, D. Serebryakov¹³⁹, L. Šerkšnytė⁹⁶, A. Sevcenco⁶², T.J. Shaba⁶⁷, A. Shabanov¹³⁹, A. Shabetai¹⁰³, R. Shahoyan³², W. Shaikh⁹⁹, A. Shangaraev¹³⁹, A. Sharma⁹⁰, D. Sharma⁴⁶, H. Sharma¹⁰⁶, M. Sharma⁹¹, N. Sharma⁹⁰, S. Sharma⁹¹, U. Sharma⁹¹, A. Shatat⁷², O. Sheibani¹¹³, K. Shigaki⁹³, M. Shimomura⁷⁷, S. Shirinkin¹³⁹, Q. Shou³⁹, Y. Sibiriak¹³⁹, S. Siddhanta⁵¹, T. Siemiarczuk⁷⁹, T.F. Silva¹⁰⁹, D. Silvermyr⁷⁵, T. Simantathammakul¹⁰⁴, R. Simeonov³⁶, G. Simonetti³², B. Singh⁹¹, B. Singh⁹⁶, R. Singh⁸⁰, R. Singh⁹¹, R. Singh⁴⁷, V.K. Singh¹³¹, V. Singhal¹³¹, T. Sinha⁹⁹, B. Sitar¹², M. Sitta^{129,55}, T.B. Skaali¹⁹, G. Skorodumovs⁹⁵, M. Slupecki⁴³, N. Smirnov¹³⁶, R.J.M. Snellings⁵⁸, E.H. Solheim¹⁹, C. Soncco¹⁰¹, J. Song¹¹³, A. Songmoolnak¹⁰⁴, F. Soramel²⁷, S. Sorensen¹¹⁹, R. Spijkers⁸⁴, I. Sputowska¹⁰⁶, J. Staa⁷⁵, J. Stachel⁹⁵, I. Stan⁶², P.J. Steffanic¹¹⁹, S.F. Stiefelmaier⁹⁵, D. Stocco¹⁰³, I. Storehaug¹⁹, M.M. Storevdt³⁴, P. Stratmann¹³⁴, S. Strazzi²⁵, C.P. Stylianidis⁸⁴, A.A.P. Suaide¹⁰⁹, C. Suire⁷², M. Sukhanov¹³⁹, M. Suljic³², V. Sumberia⁹¹, S. Sumowidagdo⁸², S. Swain⁶⁰, A. Szabo¹², I. Szarka¹², U. Tabassam¹³, S.F. Taghavi⁹⁶, G. TAILLEPIED^{98,124}, J. Takahashi¹¹⁰, G.J. Tambave²⁰, S. Tang^{124,6}, Z. Tang¹¹⁷, J.D. Tapia Takaki¹¹⁵, N. Tapus¹²³, L.A. Tarasovicova¹³⁴, M.G. Tarzila⁴⁵, A. Tauro³², A. Telesca³², L. Terlizzi²⁴, C. Terrevoli¹¹³, G. Tersimonov³, S. Thakur¹³¹, D. Thomas¹⁰⁷, R. Tieulent¹²⁵, A. Tikhonov¹³⁹, A.R. Timmins¹¹³, M. Tkacik¹⁰⁵, T. Tkacik¹⁰⁵, A. Toia⁶³, N. Topilskaya¹³⁹, M. Toppi⁴⁸, F. Torres-Acosta¹⁸, T. Tork⁷², A.G. Torres Ramos³¹, A. Trifiró^{30,52}, A.S. Triolo^{30,52}, S. Tripathy⁵⁰, T. Tripathy⁴⁶, S. Trogolo³², V. Trubnikov³, W.H. Trzaska¹¹⁴, T.P. Trzcinski¹³², R. Turrisi⁵³, T.S. Tveter¹⁹, K. Ullaland²⁰, B. Ulukutlu⁹⁶, A. Uras¹²⁵, M. Urioni^{54,130}, G.L. Usai²², M. Vala³⁷, N. Valle²¹, S. Vallero⁵⁵, L.V.R. van Doremalen⁵⁸, M. van Leeuwen⁸⁴, C.A. van Veen⁹⁵, R.J.G. van Weelden⁸⁴, P. Vande Vyvre³², D. Varga¹³⁵, Z. Varga¹³⁵, M. Varga-Kofarago¹³⁵, M. Vasileiou⁷⁸, A. Vasiliev¹³⁹, O. Vázquez Doce⁹⁶, V. Vechernin¹³⁹, E. Vercellin²⁴, S. Vergara Limón⁴⁴, L. Vermunt⁵⁸, R. Vértesi¹³⁵, M. Verweij⁵⁸, L. Vickovic³³, Z. Vilakazi¹²⁰, O. Villalobos Baillie¹⁰⁰, G. VINO⁴⁹, A. Vinogradov¹³⁹, T. Virgili²⁸, V. Vislavicius⁸³, A. Vodopyanov¹⁴⁰, B. Volkel³², M.A. Völkl⁹⁵, K. Voloshin¹³⁹, S.A. Voloshin¹³³, G. Volpe³¹, B. von Haller³², I. Vorobyev⁹⁶, N. Vozniuk¹³⁹, J. Vrláková³⁷, B. Wagner²⁰, C. Wang³⁹, D. Wang³⁹, M. Weber¹⁰², A. Wegrzynek³², F.T. Weiglhofer³⁸, S.C. Wenzel³², J.P. Wessels¹³⁴, S.L. Weyhmler¹³⁶, J. Wiechula⁶³, J. Wikne¹⁹, G. Wilk⁷⁹, J. Wilkinson⁹⁸, G.A. Willems¹³⁴, B. Windelband⁹⁵, M. Winn¹²⁷, J.R. Wright¹⁰⁷, W. Wu³⁹, Y. Wu¹¹⁷, R. Xu⁶, A.K. Yadav¹³¹, S. Yalcin⁷¹, Y. Yamaguchi⁹³, K. Yamakawa⁹³, S. Yang²⁰, S. Yano⁹³, Z. Yin⁶, I.-K. Yoo¹⁶, J.H. Yoon⁵⁷, S. Yuan²⁰, A. Yuncu⁹⁵, V. Zaccolo²³, C. Zampolli³², H.J.C. Zanoli⁵⁸, F. Zanone⁹⁵, N. Zardoshti^{32,100}, A. Zarochentsev¹³⁹, P. Závada⁶¹, N. Zaviyalov¹³⁹, M. Zhalov¹³⁹, B. Zhang⁶, S. Zhang³⁹, X. Zhang⁶, Y. Zhang¹¹⁷, M. Zhao¹⁰, V. Zhrebchevskii¹³⁹, Y. Zhi¹⁰, N. Zhigareva¹³⁹, D. Zhou⁶, Y. Zhou⁸³, J. Zhu^{98,6}, Y. Zhu⁶, G. Zinovjev^{1,3}, N. Zurlo^{130,54}

Affiliation Notes

- ^I Deceased
^{II} Also at: Max-Planck-Institut für Physik, Munich, Germany
^{III} Also at: Italian National Agency for New Technologies, Energy and Sustainable Economic Development (ENEA), Bologna, Italy
^{IV} Also at: Dipartimento DET del Politecnico di Torino, Turin, Italy
^V Also at: Department of Applied Physics, Aligarh Muslim University, Aligarh, India
^{VI} Also at: Institute of Theoretical Physics, University of Wrocław, Poland
^{VII} Also at: An institution covered by a cooperation agreement with CERN

Collaboration Institutes

- ¹ A.I. Alikhanyan National Science Laboratory (Yerevan Physics Institute) Foundation, Yerevan, Armenia
² AGH University of Science and Technology, Cracow, Poland
³ Bogolyubov Institute for Theoretical Physics, National Academy of Sciences of Ukraine, Kiev, Ukraine
⁴ Bose Institute, Department of Physics and Centre for Astroparticle Physics and Space Science (CAPSS), Kolkata, India
⁵ California Polytechnic State University, San Luis Obispo, California, United States
⁶ Central China Normal University, Wuhan, China
⁷ Centro de Aplicaciones Tecnológicas y Desarrollo Nuclear (CEADEN), Havana, Cuba
⁸ Centro de Investigación y de Estudios Avanzados (CINVESTAV), Mexico City and Mérida, Mexico
⁹ Chicago State University, Chicago, Illinois, United States
¹⁰ China Institute of Atomic Energy, Beijing, China
¹¹ Chungbuk National University, Cheongju, Republic of Korea
¹² Comenius University Bratislava, Faculty of Mathematics, Physics and Informatics, Bratislava, Slovak Republic
¹³ COMSATS University Islamabad, Islamabad, Pakistan
¹⁴ Creighton University, Omaha, Nebraska, United States
¹⁵ Department of Physics, Aligarh Muslim University, Aligarh, India
¹⁶ Department of Physics, Pusan National University, Pusan, Republic of Korea
¹⁷ Department of Physics, Sejong University, Seoul, Republic of Korea
¹⁸ Department of Physics, University of California, Berkeley, California, United States
¹⁹ Department of Physics, University of Oslo, Oslo, Norway
²⁰ Department of Physics and Technology, University of Bergen, Bergen, Norway
²¹ Dipartimento di Fisica, Università di Pavia, Pavia, Italy
²² Dipartimento di Fisica dell'Università and Sezione INFN, Cagliari, Italy
²³ Dipartimento di Fisica dell'Università and Sezione INFN, Trieste, Italy
²⁴ Dipartimento di Fisica dell'Università and Sezione INFN, Turin, Italy
²⁵ Dipartimento di Fisica e Astronomia dell'Università and Sezione INFN, Bologna, Italy
²⁶ Dipartimento di Fisica e Astronomia dell'Università and Sezione INFN, Catania, Italy
²⁷ Dipartimento di Fisica e Astronomia dell'Università and Sezione INFN, Padova, Italy
²⁸ Dipartimento di Fisica 'E.R. Caianiello' dell'Università and Gruppo Collegato INFN, Salerno, Italy
²⁹ Dipartimento DISAT del Politecnico and Sezione INFN, Turin, Italy
³⁰ Dipartimento di Scienze MIFT, Università di Messina, Messina, Italy
³¹ Dipartimento Interateneo di Fisica 'M. Merlin' and Sezione INFN, Bari, Italy
³² European Organization for Nuclear Research (CERN), Geneva, Switzerland
³³ Faculty of Electrical Engineering, Mechanical Engineering and Naval Architecture, University of Split, Split, Croatia
³⁴ Faculty of Engineering and Science, Western Norway University of Applied Sciences, Bergen, Norway
³⁵ Faculty of Nuclear Sciences and Physical Engineering, Czech Technical University in Prague, Prague, Czech Republic
³⁶ Faculty of Physics, Sofia University, Sofia, Bulgaria
³⁷ Faculty of Science, P.J. Šafárik University, Košice, Slovak Republic
³⁸ Frankfurt Institute for Advanced Studies, Johann Wolfgang Goethe-Universität Frankfurt, Frankfurt, Germany
³⁹ Fudan University, Shanghai, China
⁴⁰ Gangneung-Wonju National University, Gangneung, Republic of Korea
⁴¹ Gauhati University, Department of Physics, Guwahati, India

- ⁴² Helmholtz-Institut für Strahlen- und Kernphysik, Rheinische Friedrich-Wilhelms-Universität Bonn, Bonn, Germany
- ⁴³ Helsinki Institute of Physics (HIP), Helsinki, Finland
- ⁴⁴ High Energy Physics Group, Universidad Autónoma de Puebla, Puebla, Mexico
- ⁴⁵ Horia Hulubei National Institute of Physics and Nuclear Engineering, Bucharest, Romania
- ⁴⁶ Indian Institute of Technology Bombay (IIT), Mumbai, India
- ⁴⁷ Indian Institute of Technology Indore, Indore, India
- ⁴⁸ INFN, Laboratori Nazionali di Frascati, Frascati, Italy
- ⁴⁹ INFN, Sezione di Bari, Bari, Italy
- ⁵⁰ INFN, Sezione di Bologna, Bologna, Italy
- ⁵¹ INFN, Sezione di Cagliari, Cagliari, Italy
- ⁵² INFN, Sezione di Catania, Catania, Italy
- ⁵³ INFN, Sezione di Padova, Padova, Italy
- ⁵⁴ INFN, Sezione di Pavia, Pavia, Italy
- ⁵⁵ INFN, Sezione di Torino, Turin, Italy
- ⁵⁶ INFN, Sezione di Trieste, Trieste, Italy
- ⁵⁷ Inha University, Incheon, Republic of Korea
- ⁵⁸ Institute for Gravitational and Subatomic Physics (GRASP), Utrecht University/Nikhef, Utrecht, Netherlands
- ⁵⁹ Institute of Experimental Physics, Slovak Academy of Sciences, Košice, Slovak Republic
- ⁶⁰ Institute of Physics, Homi Bhabha National Institute, Bhubaneswar, India
- ⁶¹ Institute of Physics of the Czech Academy of Sciences, Prague, Czech Republic
- ⁶² Institute of Space Science (ISS), Bucharest, Romania
- ⁶³ Institut für Kernphysik, Johann Wolfgang Goethe-Universität Frankfurt, Frankfurt, Germany
- ⁶⁴ Instituto de Ciencias Nucleares, Universidad Nacional Autónoma de México, Mexico City, Mexico
- ⁶⁵ Instituto de Física, Universidade Federal do Rio Grande do Sul (UFRGS), Porto Alegre, Brazil
- ⁶⁶ Instituto de Física, Universidad Nacional Autónoma de México, Mexico City, Mexico
- ⁶⁷ iThemba LABS, National Research Foundation, Somerset West, South Africa
- ⁶⁸ Jeonbuk National University, Jeonju, Republic of Korea
- ⁶⁹ Johann-Wolfgang-Goethe Universität Frankfurt Institut für Informatik, Fachbereich Informatik und Mathematik, Frankfurt, Germany
- ⁷⁰ Korea Institute of Science and Technology Information, Daejeon, Republic of Korea
- ⁷¹ KTO Karatay University, Konya, Turkey
- ⁷² Laboratoire de Physique des 2 Infinis, Irène Joliot-Curie, Orsay, France
- ⁷³ Laboratoire de Physique Subatomique et de Cosmologie, Université Grenoble-Alpes, CNRS-IN2P3, Grenoble, France
- ⁷⁴ Lawrence Berkeley National Laboratory, Berkeley, California, United States
- ⁷⁵ Lund University Department of Physics, Division of Particle Physics, Lund, Sweden
- ⁷⁶ Nagasaki Institute of Applied Science, Nagasaki, Japan
- ⁷⁷ Nara Women's University (NWU), Nara, Japan
- ⁷⁸ National and Kapodistrian University of Athens, School of Science, Department of Physics, Athens, Greece
- ⁷⁹ National Centre for Nuclear Research, Warsaw, Poland
- ⁸⁰ National Institute of Science Education and Research, Homi Bhabha National Institute, Jatni, India
- ⁸¹ National Nuclear Research Center, Baku, Azerbaijan
- ⁸² National Research and Innovation Agency - BRIN, Jakarta, Indonesia
- ⁸³ Niels Bohr Institute, University of Copenhagen, Copenhagen, Denmark
- ⁸⁴ Nikhef, National institute for subatomic physics, Amsterdam, Netherlands
- ⁸⁵ Nuclear Physics Group, STFC Daresbury Laboratory, Daresbury, United Kingdom
- ⁸⁶ Nuclear Physics Institute of the Czech Academy of Sciences, Husinec-Řež, Czech Republic
- ⁸⁷ Oak Ridge National Laboratory, Oak Ridge, Tennessee, United States
- ⁸⁸ Ohio State University, Columbus, Ohio, United States
- ⁸⁹ Physics department, Faculty of science, University of Zagreb, Zagreb, Croatia
- ⁹⁰ Physics Department, Panjab University, Chandigarh, India
- ⁹¹ Physics Department, University of Jammu, Jammu, India
- ⁹² Physics Department, University of Rajasthan, Jaipur, India
- ⁹³ Physics Program and International Institute for Sustainability with Knotted Chiral Meta Matter (SKCM2), Hiroshima University, Hiroshima, Japan

- ⁹⁴ Physikalisches Institut, Eberhard-Karls-Universität Tübingen, Tübingen, Germany
⁹⁵ Physikalisches Institut, Ruprecht-Karls-Universität Heidelberg, Heidelberg, Germany
⁹⁶ Physik Department, Technische Universität München, Munich, Germany
⁹⁷ Politecnico di Bari and Sezione INFN, Bari, Italy
⁹⁸ Research Division and ExtreMe Matter Institute EMMI, GSI Helmholtzzentrum für Schwerionenforschung GmbH, Darmstadt, Germany
⁹⁹ Saha Institute of Nuclear Physics, Homi Bhabha National Institute, Kolkata, India
¹⁰⁰ School of Physics and Astronomy, University of Birmingham, Birmingham, United Kingdom
¹⁰¹ Sección Física, Departamento de Ciencias, Pontificia Universidad Católica del Perú, Lima, Peru
¹⁰² Stefan Meyer Institut für Subatomare Physik (SMI), Vienna, Austria
¹⁰³ SUBATECH, IMT Atlantique, Nantes Université, CNRS-IN2P3, Nantes, France
¹⁰⁴ Suranaree University of Technology, Nakhon Ratchasima, Thailand
¹⁰⁵ Technical University of Košice, Košice, Slovak Republic
¹⁰⁶ The Henryk Niewodniczanski Institute of Nuclear Physics, Polish Academy of Sciences, Cracow, Poland
¹⁰⁷ The University of Texas at Austin, Austin, Texas, United States
¹⁰⁸ Universidad Autónoma de Sinaloa, Culiacán, Mexico
¹⁰⁹ Universidade de São Paulo (USP), São Paulo, Brazil
¹¹⁰ Universidade Estadual de Campinas (UNICAMP), Campinas, Brazil
¹¹¹ Universidade Federal do ABC, Santo Andre, Brazil
¹¹² University of Cape Town, Cape Town, South Africa
¹¹³ University of Houston, Houston, Texas, United States
¹¹⁴ University of Jyväskylä, Jyväskylä, Finland
¹¹⁵ University of Kansas, Lawrence, Kansas, United States
¹¹⁶ University of Liverpool, Liverpool, United Kingdom
¹¹⁷ University of Science and Technology of China, Hefei, China
¹¹⁸ University of South-Eastern Norway, Kongsberg, Norway
¹¹⁹ University of Tennessee, Knoxville, Tennessee, United States
¹²⁰ University of the Witwatersrand, Johannesburg, South Africa
¹²¹ University of Tokyo, Tokyo, Japan
¹²² University of Tsukuba, Tsukuba, Japan
¹²³ University Politehnica of Bucharest, Bucharest, Romania
¹²⁴ Université Clermont Auvergne, CNRS/IN2P3, LPC, Clermont-Ferrand, France
¹²⁵ Université de Lyon, CNRS/IN2P3, Institut de Physique des 2 Infinis de Lyon, Lyon, France
¹²⁶ Université de Strasbourg, CNRS, IPHC UMR 7178, F-67000 Strasbourg, France, Strasbourg, France
¹²⁷ Université Paris-Saclay Centre d’Etudes de Saclay (CEA), IRFU, Département de Physique Nucléaire (DPhN), Saclay, France
¹²⁸ Università degli Studi di Foggia, Foggia, Italy
¹²⁹ Università del Piemonte Orientale, Vercelli, Italy
¹³⁰ Università di Brescia, Brescia, Italy
¹³¹ Variable Energy Cyclotron Centre, Homi Bhabha National Institute, Kolkata, India
¹³² Warsaw University of Technology, Warsaw, Poland
¹³³ Wayne State University, Detroit, Michigan, United States
¹³⁴ Westfälische Wilhelms-Universität Münster, Institut für Kernphysik, Münster, Germany
¹³⁵ Wigner Research Centre for Physics, Budapest, Hungary
¹³⁶ Yale University, New Haven, Connecticut, United States
¹³⁷ Yonsei University, Seoul, Republic of Korea
¹³⁸ Zentrum für Technologie und Transfer (ZTT), Worms, Germany
¹³⁹ Affiliated with an institute covered by a cooperation agreement with CERN
¹⁴⁰ Affiliated with an international laboratory covered by a cooperation agreement with CERN.